

Compressional modes in two-superfluid neutron stars with leptonic buoyancy

Peter B. Rau[★] and Ira Wasserman

Cornell Center for Astrophysics and Planetary Science, Cornell University, Ithaca, NY, U.S.A.

Accepted 2018 September 5. Received 2018 August 24; in original form 2018 March 1

ABSTRACT

We investigate the compressional modes of cold neutron stars with cores consisting of superfluid neutrons, superconducting protons and normal fluid electrons and muons, and crusts that contain superfluid neutrons plus a normal fluid of (spherical) nuclei and electrons. We develop a two-fluid formalism for the core that accounts for leptonic buoyancy, and an analogous treatment for the crust. We adopt the Cowling approximation, neglecting gravitational perturbations, but include all effects of the background space-time. We introduce a phenomenological, easily-modified nuclear equation of state which contains all of the thermodynamic information required to compute the coupled fluid oscillations, with parameters that are constrained by nuclear physics and the requirement that the maximum mass of a neutron star is $\geq 2M_{\odot}$. Using four parametrizations of this equation of state with nuclear compressibilities $K = 230\text{--}280$ MeV, we calculate the Brunt–Väisälä frequency due to leptonic buoyancy, and find the corresponding g -mode frequencies and eigenfunctions. We find that the WKB approximation reproduces g -mode frequencies closely. We examine the dependence of g -mode frequencies on stellar mass, nuclear compressibility and strength of neutron-proton entrainment, and compare to previous calculations of g -mode frequencies due to leptonic buoyancy. We also compute the p -mode spectra, confirming previous findings that the two fluids behave as if uncoupled except the case of large entrainment, and show the existence of nearly resonant mode pairs which could lead to nonlinear p - g instabilities even at zero temperature.

Key words: stars: neutron – stars: oscillations – equation of state

1 INTRODUCTION

The first observation of gravitational waves from a binary neutron star merger (Abbott et al. 2017) opens up the possibility of studying neutron stars interiors through tidally-induced phase shifts to gravitational waveforms (Lackey & Wade 2015; Agathos et al. 2015). This would allow gravitational wave astronomy to serve as a probe of the equation of state above nuclear density, which is otherwise difficult to study. Low-frequency modes with frequencies swept by the orbital frequency may be resonantly excited by tidal interactions in neutron star-black hole and neutron star-neutron star mergers (Bildsten & Cutler 1992; Cutler et al. 1993; Lai 1994; Reisenegger & Goldreich 1994; Xu & Lai 2017; Andersson & Ho 2018), causing a phase shift that depends on the exact nature of the excited modes. Low frequency g -modes are especially interesting, although the resulting gravitational waveform phase shifts from their resonant excitation will likely be impossible to measure with current-generation

detectors unless the merging neutron stars are rapidly rotating or have large radii (Ho & Lai 1999; Flanagan & Racine 2007). The acoustic p -modes are too high in frequency to be resonantly excited themselves, but could participate in nonlinear tidal interactions involving the coupling of the g -modes and the p -modes which may be observable through a gravitational waveform phase shift (Weinberg et al. 2013; Essick et al. 2016).

Potential sources of g -modes in neutron stars have been studied for decades. In a normal fluid neutron star, buoyancy arising from temperature gradients (McDermott et al. 1983; Bildsten & Cutler 1995) and the proton fraction gradient (Reisenegger & Goldreich 1992) have been investigated, supporting modes of frequencies $1 \sim 100$ Hz. Lee (1995) studied proton fraction gradient g -modes in Newtonian stars with superfluid cores, and confirmed a previous calculation by Lindblom & Mendell (1994) which found two sets of p -modes, corresponding to normal fluid and superfluid degree of freedom respectively. Sound speeds for both sets of superfluid neutron star p -modes have been calculated by Epstein (1988), and this second set of p -modes

[★] E-mail: pbr44@cornell.edu

has also been found in a fully relativistic, finite-temperature calculation (Gualtieri et al. 2014). However, in neutron star cores composed of superfluid neutrons and superfluid-superconducting protons (Lombardo & Schulze 2001; Page et al. 2011), proton fraction gradients do not lead to g -modes unless temperatures are above the neutron critical temperature, estimated to be $\lesssim 10^9$ K (Yakovlev et al. 1999), above which electron-neutron coupling (Bertoni et al. 2015) and electron-proton electrostatic coupling will cause both baryon species to move together. G -modes due to entropy gradients in superfluid neutron stars were first found by Gusakov & Kantor (2013), and shortly thereafter they found a new class of g -modes resulting from leptonic buoyancy (Kantor & Gusakov 2014) (hereafter KG14). This effect is caused by a gradient in the electron fraction at number densities $\gtrsim 0.13$ fm $^{-3}$, where both electrons and muons coexist in most equations of state. While these leptonic buoyancy g -modes were considered in a nonzero temperature star, they were found to exist even in the zero-temperature limit, and their existence was independently confirmed (Passamonti et al. 2016). A recent paper by Yu & Weinberg (2017a) (hereafter YW17) has computed g -mode frequencies and displacement fields arising from leptonic buoyancy in zero temperature neutron star cores using Newtonian gravity, and used their results to study resonant tidal excitation of the modes during neutron star binary inspiral.

We calculate both sets of compressional modes of two-superfluid neutron stars in the zero-temperature approximation, including both the g -modes arising due to leptonic buoyancy and the p -modes, but with a few crucial differences to previous calculations. Like KG14, we include general relativity and work in the Cowling approximation, neglecting the effects of perturbations to the metric; YW17 used Newtonian gravity but included self gravity perturbations. Secondly, we use a flexible parametrized equation of state (EOS) that allows us to easily adjust the compressibility of the neutron star core, and employ this EOS to calculate the g -modes for a range of compressibilities and correspondingly a range of stellar masses and radii. Thirdly, we allow the neutron superfluid to flow into the crust of normal fluid nuclei instead of assuming that the crust is a single normal fluid. We find that this has important implications for the neutron component of the g -modes and for both components of the p -modes. We compute the displacement fields for the g -modes, which KG14 did not report in their initial letter but YW17 did, although the differences in our method mentioned above mean that our modes differ qualitatively and quantitatively. We also use our formalism to compute the p -modes in the star like Lee (1995) and Gualtieri et al. (2014), though only in the zero temperature limit.

In Section 2, we introduce the parametrized equation of state we use in the core (Section 2.1) and the crust (Section 2.2). In Section 3 we obtain the equations of motion for the modes and compute the Brunt–Väisälä frequency due to the muon gradient in the core. The crust-core interface and boundary conditions for the modes, which we find are significant to determining the normal mode displacement fields, are then discussed. Finally, in Section 4 we compute the g - and p -modes, with and without entrainment of the superfluid neutrons and protons in the core, and we make comparisons to previous calculations.

2 EQUATION OF STATE

Here we describe the model of the background neutron star that we used for the calculation of the Brunt–Väisälä frequency in Section 3.2 and the compressional modes in Section 4. Our EOS is based on a relatively simple, parametrized model. We adopt parameters to satisfy constraints near nuclear density $n_{\text{nuc}} = 0.16$ fm $^{-3}$ and allow neutron star masses above $2M_{\odot}$. It is a phenomenological model, but is sufficiently detailed that we can compute all thermodynamic quantities we need to find the normal modes. $\hbar = c = 1$ is used throughout.

2.1 Core equation of state

We consider an electrically neutral fluid of neutrons, protons, electrons and muons at zero temperature. Its energy density ρ is specified as a function of three variables: baryon number density n_{b} , proton fraction Y and electron fraction f , where the neutron, proton, electron and muon number densities are respectively $n_{\text{n}} = n_{\text{b}}(1 - Y)$, $n_{\text{p}} = n_{\text{b}}Y$, $n_{\text{e}} = n_{\text{b}}Yf$ and $n_{\mu} = n_{\text{b}}Y(1 - f)$. We separate the energy density into kinetic and interaction parts $\rho = \rho_{\text{kin}} + \rho_{\text{int}}$; the kinetic part (including the rest mass) is given by

$$\rho_{\text{kin}}(n_{\text{b}}, Y, f) = \frac{p_{\text{Fe}}^4}{4\pi^2} + \sum_{j=\text{n,p},\mu} \frac{m_j^4}{\pi^2} \phi\left(\frac{p_{\text{F}j}}{m_j}\right) \quad (1)$$

for Fermi momenta $p_{\text{F}j} = (3\pi^2 n_j)^{1/3}$ and bare mass m_j of particle species j , and where

$$\phi(x) = \frac{x^3}{4} \sqrt{x^2 + 1} + \frac{x}{8} \sqrt{x^2 + 1} - \frac{1}{8} \operatorname{arsinh}(x). \quad (2)$$

We have assumed the electrons are ultrarelativistic and ignore the difference between the proton and neutron mass, assuming $m_{\text{n}} = m_{\text{p}} = m_{\text{N}}$. Although we use the bare nucleon mass, we assume that ρ_{int} includes effective mass corrections adequately. The interaction energy density $\rho_{\text{int}}(n_{\text{b}}, Y)$ employed is based on that of Hebel et al. (2013), but with a different form for the symmetry penalty term:

$$\rho_{\text{int}}(n_{\text{b}}, Y) = n_{\text{nuc}} E_{\text{S}} \frac{\bar{n}^2 + f_{\text{S}} \bar{n}^{\gamma_{\text{S}} + 1}}{1 + f_{\text{S}}} + n_{\text{nuc}} E_{\text{A}} \bar{n}^2 \left(\frac{\bar{n} + \bar{n}_0}{1 + \bar{n}_0} \right)^{\gamma_{\text{A}} - 1} (1 - 2Y)^2, \quad (3)$$

where $\bar{n} = n_{\text{b}}/n_{\text{nuc}}$ and \bar{n}_0 is a characteristic number density. For $\bar{n} \ll \bar{n}_0$, the symmetry penalty term is quadratic in \bar{n} , as the energy per baryon should be linear in the density at low densities.

The requirements of -16 MeV per baryon binding energy and zero pressure for symmetric nuclear matter at nuclear density constraint the parameters E_{S} , γ_{S} and f_{S} , while experimental measurements like those used in constructing Figure 6 of Lattimer & Prakash (2016) constrain E_{A} , γ_{A} and \bar{n}_0 . Another constraint is that the EOS must allow a maximum mass $\geq 2M_{\odot}$ (Antoniadis et al. 2013), though this can be adjusted upward to allow for higher masses if required by future observations. We consider four possible parameter choices PC1–PC4, differing in the values of γ_{S} and f_{S} , with each choice corresponding to a value of the nuclear compressibility parameter $K = 9(\partial^2(\rho/n_{\text{b}})/\partial \bar{n}^2)|_{\bar{n}=1, Y=1/2}$. These are listed in Table 1. For these choices of E_{A} , γ_{A} and \bar{n}_0 ,

Table 1. Different parametrizations of core equation of state and corresponding nuclear compressibility K , maximum mass M_{\max} , radius at maximum mass R_{\max} , central baryon number density for the maximum mass star $n_{b,\text{cntr,max}}$ and the baryon number density at which the sound speed equals the speed of light $n_{b,\text{cl}}$.

	PC1	PC2	PC3	PC4
E_S (MeV)	-37.8	-37.8	-37.8	-37.8
γ_S	1.31	1.356	1.452	1.547
f_S	-0.667	-0.634	-0.577	-0.530
E_A (MeV)	19.9	19.9	19.9	19.9
γ_A	0.61	0.61	0.61	0.61
\bar{n}_0 (MeV)	0.05	0.05	0.05	0.05
K (MeV)	230	240	260	280
M_{\max}/M_{\odot}	2.01	2.05	2.15	2.24
R_{\max} (km)	10.23	10.34	10.62	10.88
$n_{b,\text{cntr,max}}/n_{\text{nuc}}$	7.43	7.22	6.73	6.32
$n_{b,\text{cl}}/n_{\text{nuc}}$	9.8	8.9	7.5	6.4

the symmetry energy $S_V = 31.73$ MeV and density derivative $L = 60.32$ MeV, within the 1σ confidence region of Figure 6 of Lattimer & Prakash (2016). Three of the chosen values of K are within the 240 ± 20 MeV confidence range cited in Lattimer & Prakash (2016), with $K = 220$ MeV not being used due to not allowing a $2M_{\odot}$ star to exist in our EOS. The $K = 280$ MeV parametrization represents a causal limit i.e. the sound speed equals the speed of light for central densities just beyond that which has the maximum mass for this parametrization. While the EOS is flexible, we found that it was difficult to obtain a maximum mass greater than $2.2M_{\odot}$, and also found that adjusting the parameters E_A , γ_A and \bar{n}_0 had only a small effect on the nuclear compressibility, so these parameters were fixed for all four parameter sets.

The pressure is specified by

$$P = n_b \frac{\partial \rho}{\partial n_b} - \rho \quad (4)$$

and the chemical potential by

$$\mu = \frac{\partial \rho}{\partial n_b}. \quad (5)$$

The individual chemical potentials are calculated using

$$\mu_x = \frac{\partial \rho}{\partial n_x}, \quad x = n, p, e, \mu. \quad (6)$$

The background star is assumed to be in beta equilibrium, implying

$$\mu_n = \mu_p + \mu_e = \mu_p + \mu_{\mu} \Rightarrow \mu_e = \mu_{\mu}. \quad (7)$$

We find that muons first appear at $n_b = 0.8n_{\text{nuc}}$ for all four EOS parametrizations that we considered. In Figure 1 (top), we compare our $\rho(n_b)$ in the core to the BSk19–BSk21 EOSs from Potekhin et al. (2013), finding that ours is in good agreement with all three of their EOSs in the lower half of the density range and with the BSk19 and BSk20 EOS in the higher density region. We also plot the proton fraction Y and $Y_e = fY$ as functions of n_b in the core (bottom).

2.2 Crust equation of state

In the inner crust between neutron drip at $n_b \sim 10^{11}$ g/cm³ and the transition to the core at $\sim 10^{14}$ g/cm³ ($n_b \sim 0.5n_{\text{nuc}}$), neutron stars are expected to consist of neutron-rich nuclei

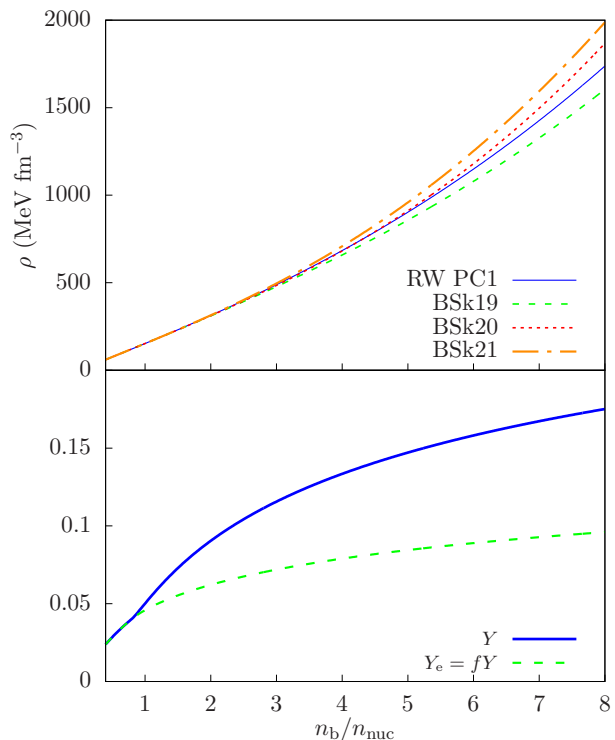


Figure 1. Top: Energy density ρ as a function of n_b/n_{nuc} in the core from this paper (RW with PC1 parameters) and the BSk19–BSk21 EOS from Potekhin et al. (2013). Bottom: Proton fraction $Y = n_p/n_b$ and electron fraction $Y_e = fY = n_e/n_b$ in the core for the RW EOS with PC1 parameters. $Y = Y_e$ below the muon threshold density $n_b/n_{\text{nuc}} = 0.8$.

surrounded by a dripped neutron gas and a pervasive ultrarelativistic electron gas. Below neutron drip, the outer crust, consisting only of nuclei and an electron gas, is included using the BPS EOS (Baym et al. 1971a). It is, however, neglected when computing the oscillation modes as it constitutes less than a hundredth of a percent of the star by mass, thus having a negligible effect on the bulk oscillation modes. The effects of this omission are briefly discussed at the conclusion of Section 3.5.

Following Baym et al. (1971b) and Haensel (2001), we consider a liquid drop-type model with spherical nuclei of radius r_n inside spherical unit cells of radius r_c . We do not model exotic shapes or nuclear pasta (Ravenhall et al. 1983a; Hashimoto et al. 1984; Watanabe et al. 2003) at this stage, and we allow the proton and nucleon numbers Z and A to vary continuously. The density of neutrons outside the nuclei is $n_{n,o}$, while the nuclei themselves have baryon density n_i . The neutron and proton densities inside the nuclei are $n_{n,i} = (1 - Y)n_i$ and $n_{p,i} = Yn_i$ respectively, where in the crust $Y = Z/A$ is the proton fraction of the nuclei and Z and A are defined to include only baryons inside the nuclei. The electron number density is fixed by electric charge neutrality to be equal to the average proton number density over the cell, so

$$n_e = wn_{p,i} = wn_i Y, \quad (8)$$

where $w = (r_n/r_c)^3$ is the fraction of the volume of each cell

occupied by the nucleus and $r_n = (3A/4\pi n_i)^{1/3}$. We also define the number density of nuclei n_n , which is given in terms of the cell radius by

$$n_n = \frac{3}{4\pi r_c^3}, \quad (9)$$

so the total baryon number density n_b is given by

$$n_b = An_n + (1-w)n_{n,o}. \quad (10)$$

Later, we discuss the fluid oscillations in the crust in terms of the macroscopic motion of two fluids: a free neutron superfluid and a normal fluid of nuclei. In the fluid equations, we use the mean density of free neutrons outside the nuclei $n_f \equiv (1-w)n_{n,o}$ and the mean density of nuclear baryons $n_c \equiv An_n$. In terms of these densities, the total baryon number density is

$$n_b = n_f + n_c; \quad (11)$$

note too that $w = n_c/n_i$.

We write the energy density for the inner crust in terms of the five variables n_f , n_c , n_i , A and Y . The energy density for the inner crust has five components: bulk energy densities for the nuclei $\rho_{i,\text{bulk}}$, surrounding neutron gas $\rho_{o,\text{bulk}}$, and electron gas ρ_e , Coulomb energy density ρ_{Coul} including the self-energy of the nuclei and the lattice energy, and surface energy density ρ_{surf} . The bulk energy density for nuclear matter, the neutron gas and the electron gas have the same form as in the core, discussed in the previous section. We then have

$$\begin{aligned} \rho(n_f, n_c, A, Y, n_i) = & w\rho_{i,\text{bulk}}(n_i, Y) + (1-w)\rho_{o,\text{bulk}}(n_f/(1-w)) \\ & + \rho_e(Yn_c) + n_n E_{\text{Coul}}(n_c, n_i, A, Y) \\ & + n_n E_{\text{surf}}(n_i, A, Y), \end{aligned} \quad (12)$$

where

$$\begin{aligned} \rho_{i,\text{bulk}}(n_i, Y) = & \frac{m_N^4}{\pi^2} \left[\phi \left(\frac{p_{\text{Fi}}}{m_N} Y^{1/3} \right) + \phi \left(\frac{p_{\text{Fi}}}{m_N} (1-Y)^{1/3} \right) \right] \\ & + n_{\text{nuc}} E_S \frac{\bar{n}_i^2 + f_S \bar{n}_i^{\gamma_S+1}}{1+f_S} + n_{\text{nuc}} E_A \bar{n}_i^2 \left(\frac{\bar{n}_i + \bar{n}_o}{1+\bar{n}_o} \right)^{\gamma_A-1} (1-2Y)^2, \end{aligned} \quad (13)$$

$$\begin{aligned} \rho_{o,\text{bulk}}(n_{n,o}) = & \frac{m_N^4}{\pi^2} \phi \left(\frac{p_{\text{Fo}}}{m_N} \right) + n_{\text{nuc}} E_S \frac{\bar{n}_{n,o}^2 + f_S \bar{n}_{n,o}^{\gamma_S+1}}{1+f_S} \\ & + n_{\text{nuc}} E_A \bar{n}_{n,o}^2 \left(\frac{\bar{n}_{n,o} + \bar{n}_o}{1+\bar{n}_o} \right)^{\gamma_A-1}, \end{aligned} \quad (14)$$

$$\rho_e(Yn_c = n_e) = \frac{(3\pi^2 n_e)^{4/3}}{4\pi^2}, \quad (15)$$

$$E_{\text{Coul}}(n_c, n_i, A, Y) = \frac{16}{15} (\pi Y n_i e)^2 r_n^5 \left[1 - \frac{3}{2} w^{1/3} + \frac{1}{2} w \right], \quad (16)$$

$$E_{\text{surf}}(n_i, A, Y) = 4\pi r_n^2 \sigma_s(Y), \quad (17)$$

where $p_{\text{Fi}} = (3\pi^2 n_i)^{1/3}$, $n_{n,o} = n_f/(1-w)$, $p_{\text{Fo}} = (3\pi^2 n_{n,o})^{1/3}$, $\bar{n}_i = n_i/n_{\text{nuc}}$, $\bar{n}_{n,o} = n_{n,o}/n_{\text{nuc}}$ and σ_s denotes the nuclear surface energy. We assume that the electrons are relativistic down to neutron drip and ignore the neutron-proton mass difference here.

Following [Ravenhall et al. \(1983b\)](#) and [Lattimer et al. \(1985\)](#), we take the surface energy σ_s to be a function only of the proton fraction Y at zero temperature, and use the

parametrization

$$\sigma_s(Y) = \frac{\sigma_0(2^{\alpha+1} + \beta)}{Y^{-\alpha} + (1-Y)^{-\alpha}}. \quad (18)$$

We selected parameters σ_0 , α , β which give a approximately constant proton number $Z \approx 40$ throughout the density range of the inner crust, as is found in more detailed calculations of the inner crust equation of state ([Douchin & Haensel 2000](#); [Onsi et al. 2008](#); [Pearson et al. 2012](#); [Potekhin et al. 2013](#)):

$$\sigma_0 = 1.4 \text{ MeV/fm}^2,$$

$$\alpha = 3,$$

$$\beta = 24.$$

α and β are close to the corresponding parameters in [Ravenhall et al. \(1983b\)](#), but σ_0 is $\approx 50\%$ larger than its corresponding parameter.

For a general change of state, the change in the energy density is

$$\begin{aligned} d\rho = & \frac{\partial \rho}{\partial A} \Big|_{n_f, n_c, n_i, Y} dA + \frac{\partial \rho}{\partial Y} \Big|_{n_f, n_c, n_i, A} dY \\ & + \frac{\partial \rho}{\partial n_i} \Big|_{n_f, n_c, A, Y} dn_i + \frac{\partial \rho}{\partial n_c} \Big|_{n_f, n_i, A, Y} dn_c \\ & + \frac{\partial \rho}{\partial n_f} \Big|_{n_c, n_i, A, Y} dn_f. \end{aligned} \quad (19)$$

At fixed n_b , $dn_c + dn_f = 0$, so this becomes

$$\begin{aligned} d\rho = & \frac{\partial \rho}{\partial A} \Big|_{n_f, n_c, n_i, Y} dA + \frac{\partial \rho}{\partial Y} \Big|_{n_f, n_c, n_i, A} dY \\ & + \frac{\partial \rho}{\partial n_i} \Big|_{n_f, n_c, A, Y} dn_i + \left(\frac{\partial \rho}{\partial n_c} \Big|_{n_f, n_i, A, Y} - \frac{\partial \rho}{\partial n_f} \Big|_{n_c, n_i, A, Y} \right) dn_c. \end{aligned} \quad (20)$$

The ‘‘nuclear virial theorem’’ ([Haensel 2001](#)) and pressure balance correspond to the conditions

$$\frac{\partial \rho}{\partial Y} \Big|_{n_f, n_c, n_i, A} = \frac{\partial \rho}{\partial n_i} \Big|_{n_f, n_c, A, Y} = 0, \quad (21)$$

respectively, while the condition that there is no energy associated with exchanging neutrons between the nuclei and the external free neutron gas (henceforth the ‘‘exchange condition’’) is

$$\frac{\partial \rho}{\partial n_c} \Big|_{n_c, n_i, A, Y} - \frac{\partial \rho}{\partial n_f} \Big|_{n_c, n_i, A, Y} - \frac{Y}{n_c} \frac{\partial \rho}{\partial Y} \Big|_{n_f, n_c, n_i, A} = 0 \quad (22)$$

since proton density Yn_c is unchanged by exchange of neutrons. Beta equilibrium is simply

$$\frac{\partial \rho}{\partial Y} \Big|_{n_f, n_c, n_i, A} = 0, \quad (23)$$

so Eq. (22) becomes

$$\frac{\partial \rho}{\partial n_c} \Big|_{n_c, n_i, A, Y} - \frac{\partial \rho}{\partial n_f} \Big|_{n_c, n_i, A, Y} = 0. \quad (24)$$

Imposing the four conditions Eqs. (21,23,24), we can determine the values of n_f , n_c , n_i , A and Y at each n_b and thus compute at each n_b the energy density ρ and pressure P , which is given by

$$P = P_e + P_{\text{Coul}} + P_{o,\text{bulk}} = \frac{1}{3}\rho_e + \frac{n_c^2}{A} \frac{\partial E_{\text{Coul}}}{\partial n_c} + P_{o,\text{bulk}}. \quad (25)$$

Table 2. Pressure P , chemical potential μ and baryon number density n_b at the core (+) and crust (-) sides of the crust-core transition for each EOS parametrization employed in this paper. The size of the density jump as a percentage of the baryon number density at the transition is also listed.

	PC1	PC2	PC3	PC4
P (MeV/fm ³)	0.215	0.225	0.239	0.249
μ/m_N	1.0108	1.0112	1.0117	1.0121
n_b^+/n_{nuc}	0.399	0.413	0.437	0.458
n_b^-/n_{nuc}	0.394	0.407	0.431	0.451
$\Delta n_b/n_b$ (%)	1.2	1.4	1.3	1.5

We will also require the chemical potentials for each fluid μ_f and μ_c , given by

$$\mu_f = \left. \frac{\partial \rho}{\partial n_f} \right|_{n_c, n_i, A, Y} = (1-w) \frac{\partial \rho_{\text{bulk}, o}}{\partial n_{n, o}} \frac{\partial n_{n, o}}{\partial n_f} = \mu_{n, o}, \quad (26)$$

$$\mu_c = \left. \frac{\partial \rho}{\partial n_c} \right|_{n_f, n_i, A, Y} = Y\mu_e + \frac{P_{o, \text{bulk}} + \rho_{\text{bulk}, i}}{n_i} + \frac{16}{15} (\pi Y n_i e)^2 \frac{Y}{A} r_n^5 \left[3 - 5w^{1/3} + 2w \right]. \quad (27)$$

Using the four equilibrium conditions, Eqs. (26–27) can be used to show that $\mu_c = \mu_f$ in equilibrium.

For this inner crust equation of state, neutron drip occurs between $2.7 - 2.8 \times 10^{11}$ g/cm³ or $n_b = 0.00103 - 0.00106 n_{\text{nuc}}$, depending on the parametrization of the nuclear physics. The core and crust equations of state must be joined when the pressure and chemical potentials of each are equal. This occurs at different densities for each EOS parametrization described in Table 1, with the pressure, chemical potential and densities in the core and crust at the transition for each parametrization listed in Table 2.

The energy density and pressure for our EOS in the crust (Figure 2), top) are within 10–20% of those found in more detailed calculations such as Pearson et al. (2012) and Potekhin et al. (2013). The bottom panel shows A , Z and n_c/n_b as functions of n_b/n_{nuc} in the crust. The values of Z closely match those of Ravenhall et al. (1972), including the dip downward just before the transition to the core. Our values of n_c/n_b are in agreement with Kobayakov & Pethick (2016); our values of A are typically greater than theirs by a factor of 1.5, though the difference increases as the crust-core transition is approached, while our values are typically a factor of 4 lower than those of Pearson et al.

Figure 3 compares the mass-radius relation for two different parametrizations of the two-part EOS described here (RW) to a few other representative neutron star equations of state. The RW EOS uses the BPS EOS (Baym et al. 1971a) for densities below neutron drip. The radius, radius at neutron drip and central density for each EOS parametrization and stellar mass used in the rest of this paper are described in Table 3.

3 FLUID DYNAMICS

3.1 Two-fluid formalism in the core

We now derive the equations of motion for the perturbations of a two-superfluid neutron star that we use to compute its normal modes. We first consider the core, and the same model is generalized to the crust in Sections (3.3) and (3.4).

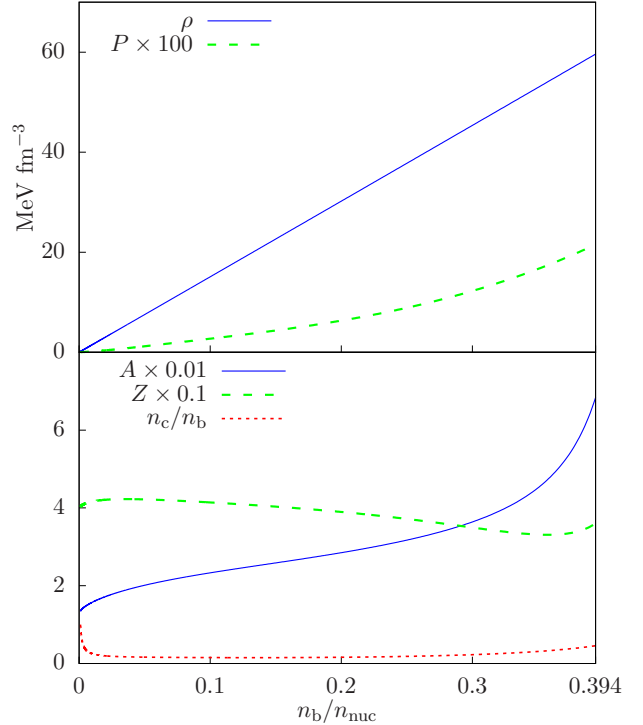


Figure 2. Top: Mass-energy density ρ and pressure P as functions of n_b/n_{nuc} across the density range of the inner crust for the RW EOS with PC1 parametrization. Bottom: Nucleon number A , proton number Z and the ratio $0 < n_c/n_b < 1$ as functions of n_b/n_{nuc} across the density range of the inner crust for the same EOS. The maximum density in the crust before the transition to the core is $n_b/n_{\text{nuc}} = 0.394$ for the PC1 parametrization.

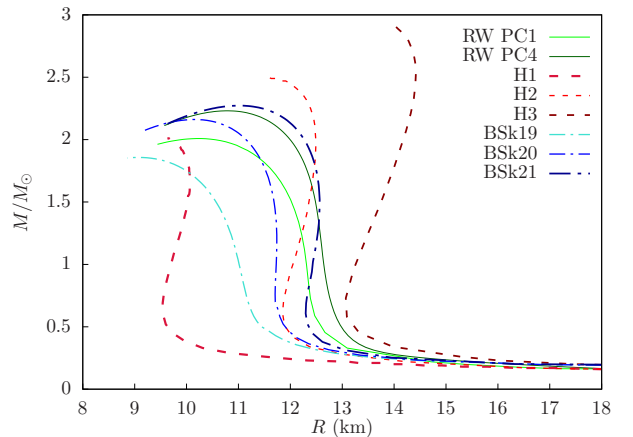


Figure 3. Neutron star mass-radius plot for the EOS described in this paper with two parametrizations as given by Table 1 (RW PC1 and RW PC4) and three equations of state of increasing stiffness from both Hebeler et al. (2013) (denoted H1, H2, H3) and Potekhin et al. (2013) (denoted BSk19, BSk20, BSk21).

Table 3. List of radius R , radius at neutron drip R_{ND} , and central density $n_{b,\text{cntr}}$ for each stellar mass and parametrization choice employed in the calculation of compressional mode frequencies in this paper.

PC1	1.2M _⊙	1.4M _⊙	1.7M _⊙	2M _⊙
R (km)	12.24	12.11	11.75	10.54
R_{ND} (km)	11.72	11.70	11.47	10.39
$n_{b,\text{cntr}}/n_{\text{nuc}}$	2.73	3.17	4.07	6.67
PC2	1.2M _⊙	1.4M _⊙	1.7M _⊙	2M _⊙
R (km)	12.31	12.21	11.90	11.06
R_{ND} (km)	11.78	11.79	11.62	10.89
$n_{b,\text{cntr}}/n_{\text{nuc}}$	2.66	3.05	3.86	5.61
PC3	1.2M _⊙	1.4M _⊙	1.7M _⊙	2M _⊙
R (km)	12.48	12.43	12.23	11.71
R_{ND} (km)	11.94	11.99	11.92	11.50
$n_{b,\text{cntr}}/n_{\text{nuc}}$	2.49	2.82	3.46	4.55
PC4	1.2M _⊙	1.4M _⊙	1.7M _⊙	2M _⊙
R (km)	12.63	12.62	12.50	12.14
R_{ND} (km)	12.07	12.17	12.17	11.92
$n_{b,\text{cntr}}/n_{\text{nuc}}$	2.35	2.64	3.16	3.96

We work at zero temperature, so there are no normal fluid neutron or proton components, and include general relativity, but work in the Cowling approximation and so ignore perturbations of the metric.

In a core composed of superfluid neutrons and protons and normal fluid electrons and muons, the leptons will move along with the protons since the plasma frequency $\sim 10^{22} \text{ s}^{-1}$ is much greater than the frequencies of the compressional modes. We thus have two independently-moving fluids—a neutron superfluid and charged fluid. This differs from the commonly-chosen separation of the fluid into normal and superfluid components, though the formulation used here has a number of advantages which illuminate the underlying physics. First, it makes clear the role of the leptonic buoyancy, which exists only in the charged fluid. It also reveals the significance of thermodynamic coupling and entrainment between the two fluids, with the equations describing the motion of the fluids becoming completely uncoupled if these quantities are zero as is demonstrated at the end of this section. At densities above $2\text{--}3n_{\text{nuc}}$, the s -wave pairing energy gap for protons may go to zero (Zhou et al. 2004; Baldo & Schulze 2007), meaning that the proton fluid can be a normal fluid in the inner core, but the equations of motion for the charged fluid will remain unchanged in this case, and the charged fluid and neutrons would still behave as two separately-moving fluids as long as the neutrons remain superfluid. Note that both methods should be equivalent, and the normal fluid and superfluid displacement modes can be reconstructed from taking the appropriate superposition of the neutron and charged fluid modes.

We assume that neutrons remain superfluid throughout the core; calculations summarized in Fig. 2 of Gezerlis et al. (2014) support the idea that the neutron gap does not vanish at any density below at least $4.2n_{\text{nuc}}$, which includes all neutron stars less massive than about $1.7M_{\odot}$ for our adopted equation of state. Moreover, these calculations suggest that neutron superfluidity would be maintained out to the crust-core boundary for core temperatures below $\approx 3 \times 10^8 \text{ K}$; the model used in KG14 is similar. If neutrons become normal somewhere inside the core, their coupling to electrons (Bertoni et al. 2015) suffices to merge

the two fluids into a single fluid, irrespective of whether the protons are superfluid. Thus, if neutrons were entirely normal throughout the core, then g -modes would arise from a combination of the leptonic buoyant force associated with the gradient of f and the buoyant force associated with the gradient of Y (Reisenegger & Goldreich 1992), but overall their frequencies would be lower than when neutrons are superfluid; see Section 3.2, especially Eqs. (82–83). However, if the neutrons are only normal deep inside the core of the neutron star, then the g -modes arising from leptonic buoyancy, which is only substantial near the outer boundary of the core, would be largely unaffected. Thus, the g -mode frequency spectrum is, in principle, a probe of neutron superfluidity in the cores of neutron stars.

We specify the neutron superfluid four-velocity u_{n}^{μ} and number density n_{n} , and charged fluid four-velocity u_{q}^{μ} and number density $n_{\text{q}} = n_{\text{p}} = n_{\text{e}} + n_{\mu}$. We can rewrite the energy density ρ as a function of n_{n} , n_{q} and the electron fraction $f = n_{\text{e}}/n_{\text{q}}$;

$$\rho(n_{\text{n}}, n_{\text{q}}, f) = \rho_{\text{nuc}}(n_{\text{n}}, n_{\text{q}}) + \rho_{\text{e}}(n_{\text{q}}f) + \rho_{\mu}(n_{\text{q}}(1-f)), \quad (28)$$

where ρ_{nuc} includes both the kinetic and interaction contributions relating to the nucleons. This gives two chemical potentials

$$\mu_{\text{n}} = \frac{\partial \rho}{\partial n_{\text{n}}} = \frac{\partial \rho_{\text{nuc}}}{\partial n_{\text{n}}}, \quad (29)$$

$$\mu_{\text{q}} = \frac{\partial \rho}{\partial n_{\text{q}}} = \frac{\partial \rho_{\text{nuc}}}{\partial n_{\text{q}}} + \frac{\partial \rho_{\text{e}}}{\partial n_{\text{e}}} \frac{\partial n_{\text{e}}}{\partial n_{\text{q}}} + \frac{\partial \rho_{\mu}}{\partial n_{\mu}} \frac{\partial n_{\mu}}{\partial n_{\text{q}}}, \quad (30)$$

which are equal in beta equilibrium.

The motion of the two fluids is described by the relativistic Euler equations (Carter & Langlois 1998; Andersson & Comer 2007)

$$0 = u_{\text{n}}^{\rho} \nabla_{\rho} (\mu_{\text{n}} u_{\text{n}}^{\sigma}) + \nabla_{\sigma} \mu_{\text{n}} - 2u_{\text{n}}^{\rho} \nabla_{[\rho} (\mu_{\text{n}} \epsilon_{\text{n}} W_{\sigma]}), \quad (31)$$

$$0 = u_{\text{q}}^{\rho} \nabla_{\rho} (\mu_{\text{q}} u_{\text{q}}^{\sigma}) + \nabla_{\sigma} \mu_{\text{q}} + (\mu_{\mu} - \mu_{\text{e}}) \nabla_{\sigma} f + 2u_{\text{q}}^{\rho} \nabla_{[\rho} (\mu_{\text{n}} \epsilon_{\text{p}} W_{\sigma]}), \quad (32)$$

and the continuity equations

$$\nabla_{\rho} (n_{\text{n}} u_{\text{n}}^{\rho}) = 0, \quad (33)$$

$$\nabla_{\rho} (n_{\text{q}} u_{\text{q}}^{\rho}) = 0. \quad (34)$$

where $W_{\sigma} = u_{\text{n}}^{\sigma} - u_{\text{q}}^{\sigma}$. ϵ_{n} and ϵ_{p} are defined to parameterize the entrainment, and are related by

$$n_{\text{q}} \epsilon_{\text{p}} = n_{\text{n}} \epsilon_{\text{n}}. \quad (35)$$

The entrainment parameters ϵ_{p} and ϵ_{n} here are dimensionless and are the same as those of Prix & Rieutord (2002). We vary the parameter ϵ_{p} to adjust the strength of the entrainment, noting that the effective mass of the proton m_{p}^* is often related to ϵ_{p} via

$$\epsilon_{\text{p}} = 1 - \frac{m_{\text{p}}^*}{m_{\text{N}}}. \quad (36)$$

The term in Eq. (32) $\propto \nabla_{\sigma} f$ is responsible for the leptonic buoyancy, and in the outer regions of the core without muons, it is zero.

We now calculate the equations of motion for perturbations to a spherically-symmetric, static background in chemical equilibrium. The metric in Schwarzschild coordinates is

$$ds^2 = -e^{\nu(r)} dt^2 + e^{\lambda(r)} dr^2 + r^2(d\theta^2 + \sin^2\theta d\phi^2), \quad (37)$$

where $e^{\lambda(r)} = (1 - 2M(r)/r)^{-1}$, $M(r)$ is the mass enclosed within radius r , and $e^{\nu(r)}$ is determined using the gravitational redshift formula $\mu(r)\sqrt{-g_{00}} = \text{constant}$, so

$$e^{\nu(r)} = (-g_{00}) = \left(\frac{m_{N,\text{Fe-56}}}{\mu_0(r)} \right)^2 \left(1 - \frac{2M}{R} \right), \quad (38)$$

where R is the coordinate radius of the star, $M = M(R)$ its total mass computed using the equation of state and the TOV equation and $m_{N,\text{Fe-56}}$ is the mass per baryon of an iron-56 nucleus.

Since the velocities under consideration are much less than the speed of light, we can ignore relativistic gamma factors and write the fluid four-velocities as

$$u_a^\mu = \frac{dx_a^\mu}{d\tau} \approx e^{-\nu/2} \frac{dx_a^\mu}{dt}. \quad (39)$$

For a stationary background, $u_a^\mu = e^{-\nu/2}(1, 0, 0, 0)$. The velocity of the perturbation δu_a^μ to first order in perturbation theory and in the Cowling approximation is thus given by (Andersson & Comer 2007)

$$\begin{aligned} \delta u_a^\mu &= (\delta_\nu^\mu + u_a^\mu u_\nu^a)(u_a^\sigma \nabla_\sigma \bar{\xi}_a^\nu - \bar{\xi}_a^\sigma \nabla_\sigma u_a^\nu) \\ &= (\delta_\nu^\mu - \delta_0^\mu \delta_\nu^0) \left(e^{-\nu/2} \nabla_0 \bar{\xi}_a^\nu - \bar{\xi}_a^\sigma \nabla_\sigma e^{-\nu/2} \delta_0^\nu \right) \end{aligned} \quad (40)$$

for Lagrangian displacement fields $\bar{\xi}_a^\mu$ defined in a coordinate basis. We set $\bar{\xi}_a^0 = 0$ using the gauge freedom within the definition of $\bar{\xi}_a^\mu$. Taking the Eulerian perturbation of Eq. (32) and considering its spatial components $\sigma = i = 1, 2, 3$, we obtain to first order in perturbation theory

$$\begin{aligned} 0 &= e^{-\nu} \partial_t^2 \bar{\xi}_q^i + e^{-\nu} \epsilon_p \partial_t^2 (\bar{\xi}_n^i - \bar{\xi}_q^i) + g^{ii} \partial_i \left(\frac{\delta \mu_q}{\mu_0} \right) \\ &\quad + \frac{(\delta \mu_\mu - \delta \mu_e)}{\mu_0} g^{ii} \partial_i f, \end{aligned} \quad (41)$$

$$0 = e^{-\nu} \partial_t^2 \bar{\xi}_n^i + e^{-\nu} \epsilon_n \partial_t^2 (\bar{\xi}_q^i - \bar{\xi}_n^i) + g^{ii} \partial_i \left(\frac{\delta \mu_n}{\mu_0} \right), \quad (42)$$

where μ_0 is the common background equilibrium chemical potential. The perturbed continuity equations are identical:

$$\delta n_a = -n_a \Theta_a - \bar{\xi}_a^r \frac{dn_a}{dr}, \quad (43)$$

where we have defined

$$\Theta_a = \frac{1}{\sqrt{-g}} \frac{\partial(\sqrt{-g} \bar{\xi}_a^i)}{\partial x^i}. \quad (44)$$

Since we consider nonrotating stars, spherical symmetry is preserved and the normal modes are spheroidal/poloidal. The displacement field for such a mode in the orthonormal tetrad is

$$\xi_a = e^{i\omega t} \left[\xi_a^r(r) Y_{lm}(\theta, \phi) \hat{e}_r + \xi_a^\perp(r) r \nabla Y_{lm}(\theta, \phi) \right] \quad a = n, q, \quad (45)$$

where $Y_{lm}(\theta, \phi)$ are the usual spherical harmonics and we use the usual orthonormal basis vectors. ω is the angular frequency of the oscillation as observed far from the star. In the coordinate basis, the components of $\bar{\xi}_a^i$ are

$$\bar{\xi}_a^r = e^{-\lambda/2} \xi_a^r(r) Y_{lm}(\theta, \phi) e^{i\omega t}, \quad (46)$$

$$\bar{\xi}_a^\theta = \xi_a^\perp(r) \frac{1}{r} \partial_\theta Y_{lm}(\theta, \phi) e^{i\omega t}, \quad (47)$$

$$\bar{\xi}_a^\phi = \xi_a^\perp(r) \frac{1}{r \sin \theta} \partial_\phi Y_{lm}(\theta, \phi) e^{i\omega t}. \quad (48)$$

To compute the buoyant term in Eq. (41), use

$$\frac{\partial \rho}{\partial f} = \frac{\partial \rho_e}{\partial n_e} \frac{\partial n_e}{\partial f} + \frac{\partial \rho_\mu}{\partial n_\mu} \frac{\partial n_\mu}{\partial f} = n_q(\mu_e - \mu_\mu); \quad (49)$$

then

$$\begin{aligned} \delta \mu_\mu - \delta \mu_e &= -\delta \left(\frac{1}{n_q} \frac{\partial \rho}{\partial f} \right) \\ &= -\frac{1}{n_q} \left(\frac{\partial^2 \rho}{\partial f^2} \delta f + \frac{\partial \mu_q}{\partial f} \delta n_q \right) \\ &= \mu_{\text{qf}} \Theta_{\text{q}}, \end{aligned} \quad (50)$$

where we have defined the thermodynamic derivatives

$$\mu_{ab} \equiv \frac{\partial \mu_a}{\partial n_b} \quad a, b \in \{n, q\}; \quad \mu_{\text{qf}} \equiv \frac{\partial \mu_q}{\partial f}, \quad (51)$$

where $\mu_{nq} = \mu_{qn}$; explicitly,

$$\mu_n = \frac{\partial \rho}{\partial n_b} - \frac{Y}{n_b} \frac{\partial \rho}{\partial Y}, \quad (52)$$

$$\mu_q = \frac{\partial \rho}{\partial n_b} + \frac{(1-Y)}{n_b} \frac{\partial \rho}{\partial Y}, \quad (53)$$

$$\mu_{nn} = \frac{\partial^2 \rho}{\partial n_b^2} - \frac{2Y}{n_b} \frac{\partial^2 \rho}{\partial n_b \partial Y} + \frac{Y^2}{n_b^2} \frac{\partial^2 \rho}{\partial Y^2}, \quad (54)$$

$$\mu_{qq} = \frac{\partial^2 \rho}{\partial n_b^2} + \frac{2(1-Y)}{n_b} \frac{\partial^2 \rho}{\partial n_b \partial Y} + \frac{(1-Y)^2}{n_b^2} \frac{\partial^2 \rho}{\partial Y^2}, \quad (55)$$

$$\mu_{nq} = \frac{\partial^2 \rho}{\partial n_b^2} + \frac{(1-2Y)}{n_b} \frac{\partial^2 \rho}{\partial n_b \partial Y} - \frac{Y(1-Y)}{n_b^2} \frac{\partial^2 \rho}{\partial Y^2}. \quad (56)$$

Henceforth, we define

$$\Pi_a = \Pi_a(r) Y_{lm}(\theta, \phi) \equiv \frac{\delta \mu_a}{\mu_0}, \quad (57)$$

in terms of which the Euler equations are

$$\omega^2 e^{-\nu} (1 - \epsilon_n) \xi_n^r + \omega^2 e^{-\nu} \epsilon_n \xi_q^r = e^{-\lambda/2} \frac{d\Pi_n}{dr}, \quad (58)$$

$$\omega^2 e^{-\nu} r (1 - \epsilon_n) \xi_n^\perp + \omega^2 e^{-\nu} r \epsilon_n \xi_q^\perp = \Pi_n, \quad (59)$$

$$\omega^2 e^{-\nu} (1 - \epsilon_p) \xi_q^r + \omega^2 e^{-\nu} \epsilon_p \xi_n^r = e^{-\lambda/2} \frac{d\Pi_q}{dr} + e^{-\lambda/2} \frac{\mu_{\text{qf}}}{\mu_0} \frac{df}{dr} \Theta_{\text{q}}, \quad (60)$$

$$\omega^2 e^{-\nu} r (1 - \epsilon_p) \xi_q^\perp + \omega^2 e^{-\nu} r \epsilon_p \xi_n^\perp = \Pi_q. \quad (61)$$

We also recast the continuity equations in terms of ξ_a^r and Π_a ; using

$$\Theta_a = \left(\frac{e^{-\lambda/2}}{r^2} \frac{d(r^2 \xi_a^r)}{dr} - \frac{l(l+1)}{r} \xi_a^\perp \right) Y_{lm}, \quad (62)$$

we obtain

$$\begin{aligned} \delta n_n(r) &= -n_n \left[\frac{e^{-\lambda/2}}{r^2} \frac{d(r^2 \xi_n^r)}{dr} - e^\nu \frac{k_\perp^2}{\omega^2} \{ (1+x) \Pi_n - x \Pi_q \} \right] \\ &\quad - e^{-\lambda/2} \xi_n^r \frac{dn_n}{dr}, \end{aligned} \quad (63)$$

$$\begin{aligned} \delta n_q(r) &= -n_q \left[\frac{e^{-\lambda/2}}{r^2} \frac{d(r^2 \xi_q^r)}{dr} - e^\nu \frac{k_\perp^2}{\omega^2} \{ (1+y) \Pi_q - y \Pi_n \} \right] \\ &\quad - e^{-\lambda/2} \xi_q^r \frac{dn_q}{dr}, \end{aligned} \quad (64)$$

where $k_{\perp}^2 \equiv l(l+1)r^{-2}$ and

$$x \equiv \frac{\epsilon_n}{1 - \epsilon_p - \epsilon_n}, \quad (65)$$

$$y \equiv \frac{\epsilon_p}{1 - \epsilon_p - \epsilon_n}. \quad (66)$$

Using

$$\delta\mu_n = \mu_{nn}\delta n_n + \mu_{nq}\delta n_q, \quad (67)$$

$$\delta\mu_q = \mu_{qq}\delta n_q + \mu_{nq}\delta n_n + \mu_{qf}\delta f, \quad (68)$$

we find

$$\delta n_n(r) = \frac{\mu_{qq}\mu_0\Pi_n - \mu_{nq}\mu_0\Pi_q - \mu_{nq}\mu_{qf}\xi_q^r(df/dr)}{D}, \quad (69)$$

$$\delta n_q(r) = \frac{\mu_{nn}\mu_0\Pi_q - \mu_{nq}\mu_0\Pi_n + \mu_{nn}\mu_{qf}\xi_q^r(df/dr)}{D}, \quad (70)$$

where $D \equiv (\mu_{nn}\mu_{qq} - \mu_{nq}^2)$; then Eq. (63–64) are

$$\begin{aligned} \frac{d\xi_n^r}{dr} + \left[\frac{2}{r} + \frac{d \ln n_n}{dr} \right] \xi_n^r + \left[-\frac{k_{\perp}^2}{\omega^2} e^{v+\lambda/2}(1+x) + \frac{\mu_0\mu_{qq}}{n_n D} e^{\lambda/2} \right] \Pi_n \\ = \left[-\frac{k_{\perp}^2}{\omega^2} e^{v+\lambda/2} x + \frac{\mu_0\mu_{nq}}{n_n D} e^{\lambda/2} \right] \Pi_q + \frac{\mu_{nq}\mu_{qf}}{n_n D} \frac{df}{dr} \xi_q^r, \end{aligned} \quad (71)$$

$$\begin{aligned} \frac{d\xi_q^r}{dr} + \left[\frac{2}{r} + \frac{d \ln n_q}{dr} + \frac{\mu_{nn}\mu_{qf}}{n_q D} \frac{df}{dr} \right] \xi_q^r \\ + \left[-\frac{k_{\perp}^2}{\omega^2} e^{v+\lambda/2}(1+y) + \frac{\mu_0\mu_{nn}}{n_q D} e^{\lambda/2} \right] \Pi_q \\ = \left[-\frac{k_{\perp}^2}{\omega^2} e^{v+\lambda/2} y + \frac{\mu_0\mu_{nq}}{n_q D} e^{\lambda/2} \right] \Pi_n. \end{aligned} \quad (72)$$

Notice that, in the case of zero entrainment and zero thermodynamic coupling $\mu_{nq} = 0$, the two equations describing the neutron fluid motion (58) and (60) are completely uncoupled from those describing the charged fluid motion (71) and (72), leading to two sets of equations coupling (ξ_n^r, Π_n) and (ξ_q^r, Π_q) , respectively.

3.2 Brunt–Väisälä frequency

To determine the Brunt–Väisälä frequency, we use the radial components of the Euler equations to get

$$\begin{aligned} \omega^2 e^{-v} \frac{1}{1+y} \xi_q^r = e^{-\lambda/2} \frac{d\Pi_q}{dr} - e^{-\lambda/2} \frac{y}{1+y} \frac{d\Pi_n}{dr} \\ - e^{-\lambda/2} \frac{\mu_{qf}(\mu_{nn}\Pi_q - \mu_{nq}\Pi_n)}{n_q D} \frac{df}{dr} \\ - e^{-\lambda} \xi_q^r \frac{\mu_{qf}}{\mu_0 n_q} \frac{df}{dr} \left[\frac{dn_q}{dr} + \frac{\mu_{nn}\mu_{qf}}{D} \frac{df}{dr} \right]; \end{aligned} \quad (73)$$

Eqs. (67–70) with $\delta\mu_a = (d\mu_a/dr)\delta r$ and $\delta n_a = (dn_a/dr)\delta r$ imply

$$\frac{dn_q}{dr} + \frac{\mu_{nn}\mu_{qf}}{D} \frac{df}{dr} = \frac{\mu_{nn} - \mu_{nq}}{D} \frac{d\mu_0}{dr}, \quad (74)$$

hence

$$\begin{aligned} \xi_q^r \left[\omega^2 + e^{v-\lambda}(1+y) \left(\frac{\mu_{qf}}{\mu_0} \frac{d\mu_0}{dr} \right) \left(\frac{\mu_{nn} - \mu_{nq}}{n_q D} \right) \frac{df}{dr} \right] \\ = e^{v-\lambda/2} \left((1+y) \frac{d\Pi_q}{dr} - y \frac{d\Pi_n}{dr} \right. \\ \left. - (1+y) \frac{\mu_{qf}(\mu_{nn}\Pi_q - \mu_{nq}\Pi_n)}{n_q D} \frac{df}{dr} \right). \end{aligned} \quad (75)$$

So the square of the Brunt–Väisälä frequency is

$$N_q^2(r) = -e^{v-\lambda}(1+y) \left(\frac{\mu_{qf}}{\mu_0} \frac{d\mu_0}{dr} \right) \left(\frac{\mu_{nn} - \mu_{nq}}{n_q D} \right) \frac{df}{dr}. \quad (76)$$

This can be rewritten in a manner which eliminates the dependence on derivatives of f . Using $\mu_e = \mu_{\mu}$ in the background, we can write

$$\begin{aligned} (3\pi^2 n_e)^{1/3} = \sqrt{(3\pi^2 n_{\mu})^{2/3} + m_{\mu}^2} \\ \Rightarrow f^{2/3} - (1-f)^{2/3} = \left(\frac{m_{\mu}^3}{3\pi^2 n_q} \right)^{2/3} \end{aligned} \quad (77)$$

and

$$\frac{df}{dr} = -\frac{f^{1/3}(1-f)^{1/3}}{n_q^{5/3}[f^{1/3} + (1-f)^{1/3}]} \left(\frac{m_{\mu}^2}{(3\pi^2)^{2/3}} \right) \frac{dn_q}{dr}. \quad (78)$$

Differentiating Eq. (30) to find

$$\begin{aligned} \mu_{qf} = \frac{\partial}{\partial f} (\mu_p + f\mu_e(fn_q) + (1-f)\mu_{\mu}((1-f)n_q)) \\ = n_e \frac{d\mu_e}{dn_e} - n_{\mu} \frac{d\mu_{\mu}}{dn_{\mu}} = \frac{m_{\mu}^2}{3(3\pi^2 n_q f)^{1/3}}, \end{aligned} \quad (79)$$

we therefore have

$$\begin{aligned} \mu_{qf} \frac{df}{dr} = -\frac{m_{\mu}}{n_q} G(f) \frac{dn_q}{dr}, \\ G(f) \equiv \frac{(1-f)^{1/3}}{3} (f^{1/3} - (1-f)^{1/3}) (f^{2/3} - (1-f)^{2/3})^{1/2}. \end{aligned} \quad (80)$$

Inserting this into Eq. (74) to eliminate dn_q/dr , then using the resulting equation to eliminate $\mu_{qf}df/dr$ from Eq. (76) gives us

$$N_q^2(r) = e^{v-\lambda}(1+y) \frac{m_{\mu} G(f)(\mu_{nn} - \mu_{nq})^2 (d\mu_0/dr)^2}{\mu_0 n_q D [n_q D - \mu_{nn} m_{\mu} G(f)]}. \quad (81)$$

$N_q(r)$ is plotted in Figure (4) with zero entrainment ($y = 0$), along with the Brunt–Väisälä frequency for a normal fluid star N_{nf} , given by

$$N_{nf} = \sqrt{N_Y^2 + Y N_q^2}, \quad (82)$$

where the lepton gradient contribution is reduced by a factor of Y due to the increased inertia of moving both the protons and neutron, and where (Reisenegger & Goldreich 1992)

$$\begin{aligned} N_Y^2(r) = -e^{v-\lambda} \left(\frac{1}{\mu_0} \frac{d\mu_0}{dr} \right) \left(\frac{\mu_{bY}}{n_b \mu_{bb}} \frac{dY}{dr} + \frac{Y \mu_{qf}}{n_b \mu_{bb}} \frac{df}{dr} \right), \quad (83) \\ \mu_{bb} = Y^2 \mu_{qq} + 2Y(1-Y)\mu_{nq} + (1-Y)^2 \mu_{nn}, \\ \mu_{bY} = n_q(\mu_{qq} - \mu_{nq}) - n_n(\mu_{nn} - \mu_{nq}). \end{aligned}$$

The superfluid leptonic Brunt–Väisälä frequency is similar to that of Figure 2 of KG14, Figure 5 of Passamonti et al. (2016) and the zero entrainment results of YW17. Differences are due to differences in the equations of state used, and in the case of the YW17 results, our inclusion of general relativity in both the background star and the perturbations and our neglect of self-gravity perturbations. Figure 5 shows N_q for fixed mass $M = 1.4M_{\odot}$ using each of the four parametrizations specified by Table 1, with the peak value of N_q decreasing slightly with increasing nuclear compressibility K .

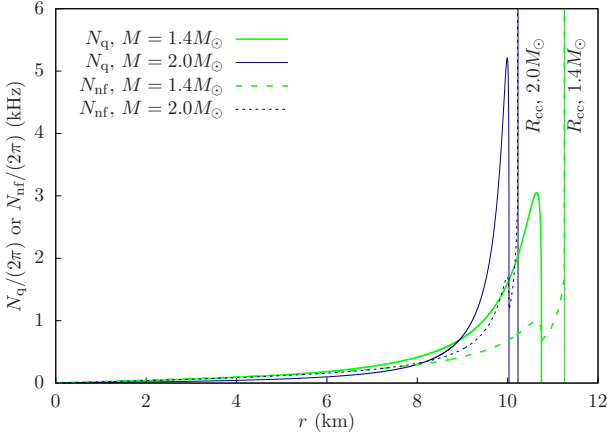


Figure 4. Brunt–Väisälä (cyclical) frequency as a function of coordinate radius r with no entrainment, calculated using the PC1 parametrization for our equation of state from Section (2) for two different model stars: $M = 1.4M_\odot$, $n_{b,\text{cntr}} = 3.17n_{\text{nuc}}$, $R = 12.11$ km, $R_{\text{cc}} = 11.27$ km and $M = 2.0M_\odot$, $n_{b,\text{cntr}} = 6.67n_{\text{nuc}}$, $R = 10.54$ km and $R_{\text{cc}} = 10.23$ km, where $n_{b,\text{cntr}}$ is the central baryon density and R_{cc} the crust-core interface radius. R_{cc} for each star is also indicated on the graph by a vertical line at the frequency cutoff for N_{nf} . The Brunt–Väisälä frequency arising due to the leptonic composition gradient in superfluid stars N_q and the total Brunt–Väisälä frequency for a normal fluid star N_{nf} are displayed. The frequency cutoffs for N_q correspond to the muon threshold, which is at the same density but a different radius for each star.

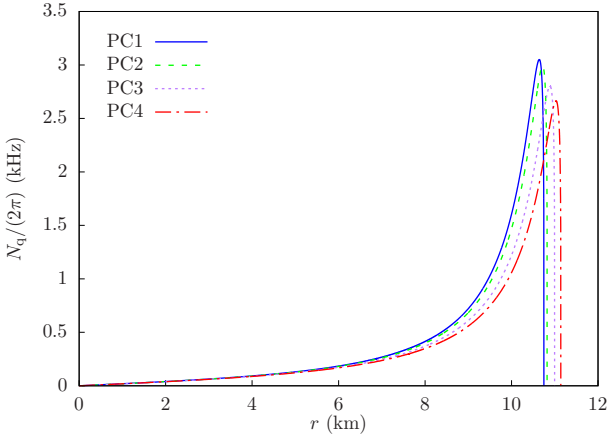


Figure 5. Brunt–Väisälä (cyclical) frequency as a function of coordinate radius r with no entrainment, for fixed mass $1.4M_\odot$ using the four EOS parametrizations specified by Table 1. The frequency cutoffs correspond to the muon threshold, which is at the same density but a different radius for each star.

Using the definition of the Brunt–Väisälä frequency, we can rewrite Eq. (60) as

$$\xi_q^r e^{-\nu} (\omega^2 - N_q^2) = e^{-\lambda/2} (1+y) \frac{d\Pi_q}{dr} - e^{-\lambda/2} y \frac{d\Pi_n}{dr} + \frac{e^{\lambda/2-\nu} \mu_0 N_q^2 (\mu_{\text{nn}} \Pi_q - \mu_{\text{nq}} \Pi_n)}{(d\mu_0/dr)(\mu_{\text{nn}} - \mu_{\text{nq}})}. \quad (84)$$

Eqs. (58), (71–72) and (84) are the four coupled first-order ODEs describing the fluid perturbations in the core.

3.3 Two-fluid formalism in the crust

To correctly calculate the compressional modes, we need to allow the oscillations in the core to propagate into the crust. As in the core, we consider two fluids– superfluid free neutrons, with displacement field $\vec{\xi}_f^i$, and normal fluid nuclei, with displacement field $\vec{\xi}_c^i$. We ignore elastic stresses here for simplicity, as we are not interested in the s (shear) and i (interface) modes caused by elasticity in the crust (McDermott et al. 1983). We also neglect entrainment, which is expected in the crust (Kobyakov & Pethick 2013; Chamel 2017) but which we do not expect to play a large role in the g -modes. Its effect on the p -modes, which we do not expect to be large either, will be examined in a later paper.

We derive the two-fluid crust equations of motion by first assuming that the perturbations of the chemical potential μ_f and μ_c in the crust can be written as a function of the two crustal number densities n_f (free neutrons) and n_c (baryons in nuclei), with changes in the other parameters of the crust EOS A , Y and n_i having been absorbed into the changes in either n_f or n_c . Thus we can write a series of four equations– the two radial and two tangential components of the perturbed Euler equations– analogously to Eqs. (58–61). We then have

$$\omega^2 e^{-\nu} \xi_f^r = e^{-\lambda/2} \frac{d\Pi_f}{dr}, \quad (85)$$

$$\omega^2 e^{-\nu} r \xi_f^\perp = \Pi_f, \quad (86)$$

$$\omega^2 e^{-\nu} \xi_c^r = e^{-\lambda/2} \frac{d\Pi_c}{dr}, \quad (87)$$

$$\omega^2 e^{-\nu} r \xi_c^\perp = \Pi_c, \quad (88)$$

where $\Pi_f \equiv \delta\mu_f/\mu_0$, $\Pi_c \equiv \delta\mu_c/\mu_0$ in analogy with Eq. (57). From the perturbed continuity equation, we also have

$$\delta n_f = -n_f \Theta_f - e^{-\lambda/2} \xi_f^r \frac{dn_f}{dr}, \quad (89)$$

$$\delta n_c = -n_c \Theta_c - e^{-\lambda/2} \xi_c^r \frac{dn_c}{dr}. \quad (90)$$

Using our assumption about the number density dependence of the perturbations, we can then rearrange

$$\delta\mu_f = \mu_{\text{ff}} \delta n_f + \mu_{\text{fc}} \delta n_c, \quad (91)$$

$$\delta\mu_c = \mu_{\text{cc}} \delta n_c + \mu_{\text{cf}} \delta n_f \quad (92)$$

to obtain

$$\delta n_f = \frac{\mu_0 (\mu_{\text{cc}} \Pi_f - \mu_{\text{fc}} \Pi_c)}{D_{\text{crust}}}, \quad (93)$$

$$\delta n_c = \frac{\mu_0 (\mu_{\text{ff}} \Pi_c - \mu_{\text{cf}} \Pi_f)}{D_{\text{crust}}}, \quad (94)$$

where $\mu_{ab} \equiv \partial\mu_a/\partial n_b$ for $a, b \in \{f, c\}$, $D_{\text{crust}} \equiv \mu_{\text{ff}} \mu_{\text{cc}} - \mu_{\text{fc}}^2$ and $\mu_0 = \mu_f = \mu_c$ in the background. There are subtleties involved in the calculation of μ_{ff} , μ_{cc} and μ_{fc} , which are discussed in Appendix A. Combining Eqs. (93–94) with

Eq. (89–90), we obtain

$$\frac{d\xi_f^r}{dr} + \left[\frac{2}{r} + \frac{d \ln n_f}{dr} \right] \xi_f^r + \left[-e^{\nu+\lambda/2} \frac{k_\perp^2}{\omega^2} + \frac{\mu_0 \mu_{cc}}{n_f D_{\text{crust}}} e^{\lambda/2} \right] \Pi_f = \frac{\mu_0 \mu_{fc}}{n_f D_{\text{crust}}} e^{\lambda/2} \Pi_c, \quad (95)$$

$$\frac{d\xi_c^r}{dr} + \left[\frac{2}{r} + \frac{d \ln n_c}{dr} \right] \xi_c^r + \left[-e^{\nu+\lambda/2} \frac{k_\perp^2}{\omega^2} + \frac{\mu_0 \mu_{ff}}{n_c D_{\text{crust}}} e^{\lambda/2} \right] \Pi_c = \frac{\mu_0 \mu_{fc}}{n_c D_{\text{crust}}} e^{\lambda/2} \Pi_f. \quad (96)$$

Eqs. (85), (87) and (95–96) are the four coupled first-order ODEs describing the fluid perturbations in the crust. Similarly to the equations in the core, in the case of zero thermodynamic coupling $\mu_{fc} = 0$, these equations become two sets of coupled equations for (ξ_f^r, Π_f) and (ξ_c^r, Π_c) .

3.4 Single normal fluid in crust

In the crust, the neutron superfluid is ${}_1S^0$, with gaps ~ 0.1 – 1 MeV until low free neutron density (Gezerlis & Carlson 2010; Gezerlis et al. 2014). Thus, we expect the free neutron gas to remain superfluid throughout most of the crust. The superfluid gap for neutrons falls precipitously at a Fermi wave number of approximately 0.05 fm^{-1} (Gezerlis et al. 2014), corresponding to a free neutron number density of $n_f = n_{\text{NF}} = 2.64 \times 10^{-5} n_{\text{nuc}}$. For our calculations, we assume that the critical temperature T_c for free crustal neutrons is purely a function of n_f . Thus, we assume that the free crustal neutrons are superfluid at $n_f > n_{\text{NF}}$ and normal at $n_f \leq n_{\text{NF}}$, so there is a sharp transition from superfluid to normal at $n_f = n_{\text{NF}}$. More realistically, T_c will also depend on n_c ; we assume that T_c depends on n_c much more weakly than it does on n_f . In a finite temperature star, the superfluid density is proportional to $T_c - T$ near the transition to normal fluid, but this temperature dependence is only important in a very thin region in the crust for T small compared with typical values of T_c in the crust, which are $\sim 10^{10}$ K.

Between the transition density and neutron drip, free neutrons and nuclei move together as a single fluid. We represent this single normal fluid, which exists only in a very thin layer just above the neutron drip density, using the displacement field ξ_b^i and the total baryon number density $n_b = n_c + n_f$. The equation of state in this region is the same as in the two-fluid region of the crust. Since the two fluids move together here, there is a buoyancy and Brunt–Väisälä frequency associated with the gradient of $Y_c \equiv n_c/n_b$.

By analogy with Eqs. (58–61), (71–72) and (84), we obtain two Euler equations and the perturbed continuity equation for the single normal fluid displacement field in the crust:

$$\omega^2 e^{-\nu} r \xi_b^i = \Pi_b, \quad (97)$$

$$\xi_b^r e^{-\nu} (\omega^2 - N_b^2) = e^{-\lambda/2} \frac{d\Pi_b}{dr} + \frac{e^{\lambda/2-\nu} \mu_0 n_b^2}{d\mu_0/dr} \Pi_b, \quad (98)$$

$$\frac{d\xi_b^r}{dr} + \left[\frac{2}{r} + \frac{d \ln n_b}{dr} + \frac{\mu_b Y_c}{n_b \mu_{bb}} \frac{dY_c}{dr} \right] \xi_b^r + \left[-e^{\nu+\lambda/2} \frac{k_\perp^2}{\omega^2} + \frac{\mu_0}{n_b \mu_{bb}} e^{\lambda/2} \right] \Pi_b = 0, \quad (99)$$

where $\Pi_b \equiv \delta\mu_b/\mu_0$ and n_b is the Brunt–Väisälä frequency associated with the gradient of Y_c , given by

$$N_b^2 = -e^{\nu-\lambda} \frac{1}{\mu_0} \frac{d\mu_0}{dr} \frac{\mu_b Y_c}{n_b \mu_{bb}} \frac{dY_c}{dr}. \quad (100)$$

The two thermodynamic derivatives μ_{bb} and $\mu_b Y_c$ are

$$\mu_{bb} = Y_c^2 \mu_{cc} + (1 - Y_c)^2 \mu_{ff} + 2Y_c(1 - Y_c) \mu_{fc}, \quad (101)$$

$$\mu_b Y_c = n_c(\mu_{cc} - \mu_{fc}) - n_f(\mu_{ff} - \mu_{fc}). \quad (102)$$

3.5 Interface and boundary conditions

At the centre of the star, we impose the regularity condition $\Theta_a = 0$, which implies that the displacement fields and Π_a satisfy the following conditions at $r = 0$:

$$\xi_a^r = l(\xi_a^r)_0 r^{l-1}, \quad (103)$$

$$\Pi_a = \omega^2 e^{-\nu} (\xi_a^r)_0 r^l, \quad (104)$$

where $(\xi_a^r)_0$ is a constant. Since we can scale the overall amplitude of each mode, we only need to specify $(\xi_n^r)_0$ and can set $(\xi_n^r)_0 = 1$.

We require four conditions at the crust-core transition which allow the computation of the four quantities $(\xi_c^r, \xi_f^r, \Pi_c, \Pi_f)$ on the crust side of the transition using the quantities $(\xi_q^r, \xi_n^r, \Pi_q, \Pi_n)$ on the core side of the transition. Since the crust-core interface is denoted by the formation of nuclei, we know that the radial component of the displacement fields for the protons must be continuous at this interface. Since the motion of the protons is described by ξ_q^i and ξ_c^i , this implies

$$(\xi_q^r)^+ = (\xi_c^r)^-, \quad (105)$$

where + indicates the high-density (core) side and – the low-density (crust) side of the transition. As baryons are not allowed to build up at the interface, baryon conservation is the second transition condition. Denoting the Lagrangian perturbation moving along with the nuclei (and hence the crust-core boundary) as Δ_c , the perturbed continuity equation for the total baryon number density is

$$\Delta_c n_b + n_b \Theta_c = 0. \quad (106)$$

Integrating this across the crust-core interface, we obtain

$$(n_n \xi_n^r - n_n \xi_q^r)^+ = (n_f \xi_f^r - n_f \xi_c^r)^-. \quad (107)$$

As we have neglected elastic stresses in the crust, continuity of the tractions across the crust-core interface is given by the continuity of the pressure perturbation moving with the interface, or

$$(\Delta_c P)^+ = (\Delta_c P)^-. \quad (108)$$

Using the Gibbs–Duhem equation, we can use $\Delta P = \sum_a n_a \Delta \mu_a$ to rewrite this condition, giving

$$(n_n \Pi_n + n_q \Pi_q)^+ = (n_c \Pi_c + n_f \Pi_f)^- + (n_b^- - n_b^+) e^{-\lambda/2} \xi_c^r \frac{d \ln \mu_0}{dr}. \quad (109)$$

Following Andersson et al. (2011) and Passamonti & Andersson (2012), the final boundary condition we impose is continuity of the neutron chemical potential perturbation, $(\Delta_c \mu_n)^+ = (\Delta_c \mu_f)^-$, which results from the “chemical gauge”-independence of the neutron chemical potential. This final interface condition simplifies to

$$(\Pi_n)^+ = (\Pi_f)^-, \quad (110)$$

where we have used $\mu_0 = \mu_c = \mu_f$ in the background equilibrium. The chemical potential is the same for crustal neutrons that are bound in nuclei or in the surrounding free superfluid; this condition is satisfied in the crustal equation of state, which allows neutrons to be exchanged freely between nuclei and the surrounding free neutron vapor (see Section 2.2 and references therein). Thus, Eq. (110) states the condition that there is no energy change when a crustal neutron is exchanged with a core neutron at the crust-core boundary irrespective of whether the crustal neutron is bound or free.

At the two fluid-single fluid transition in the crust just above neutron drip, baryon conservation and continuity of the tractions must be imposed. These two conditions can be expressed as

$$(n_f \xi_f^r + n_c \xi_c^r)^+ = (n_b \xi_b^r)^-, \quad (111)$$

$$(n_f \Pi_f + n_c \Pi_c)^+ = (n_b \Pi_b)^-, \quad (112)$$

where $+/-$ indicate the high density (two fluid) and low density (single fluid) regions respectively. We also require another boundary condition at the two fluid-single fluid transition (SFT). In a very thin region where the superfluid neutron fraction f falls from one to zero, $\xi_f^r = f \xi_{sf}^r + (1-f) \xi_{nf}^r$, where ξ_{sf}^r and ξ_{nf}^r are the radial components of the superfluid neutron and normal fluid neutron displacement fields. If the normal neutrons couple perfectly to the charged component, then $f \xi_{sf}^r = \xi_f^r - (1-f) \xi_c^r \rightarrow \xi_f^r - \xi_c^r$ for $f \rightarrow 0$. The current carried by the superfluid component should vanish where the superfluid neutrons disappear, which is true if

$$(\xi_f^r)^+ = (\xi_c^r)^+ \quad (113)$$

at the surface where $f = 0$. Combined with Eq. (111), this implies that

$$(\xi_f^r)^+ = (\xi_c^r)^+ = (\xi_b^r)^-. \quad (114)$$

A boundary condition is required at the outer surface of the star, which we approximate to occur at the neutron drip line since the outer crust contains so little of the star's mass (less than 0.01%) that we assume that its effect on the modes is negligible. We impose a form of the condition expressed in Eqs. (109), but applied to the displacement field of the single normal fluid which exists just above neutron drip (ND)

$$\left(\Pi_b + e^{-\lambda/2} \xi_b^r \frac{d \ln \mu_0}{dr} \right)_{\text{at ND}} = 0. \quad (115)$$

As a check, we also compute a few g -modes and p -modes while integrating out to lower densities in the crust, imposing Eq. (115) at $n_b/n_{\text{nuc}} = 1 \times 10^{-8}$. The g -mode frequencies obtained when doing so agree to within 0.1% of those found when we stopped the integration at neutron drip. There is no discernible change in the core displacement fields for g -modes for these two boundary conditions, and the changes in the displacement fields in the crust are larger than in the core but still very small. The p -mode frequencies obtained in this way are within 2% of those calculated with neutron drip as the stopping point for the integration. The p -mode displacement fields in the core are weakly affected by this shift in the minimum density, but the modes in the crust can differ significantly, particularly for the higher frequency modes which can have additional oscillations in the crust.

4 NORMAL MODE CALCULATIONS

4.1 WKB solutions

Since the leptonic Brunt–Väisälä frequency does not exist in the crust, we expect that the g -mode displacement fields in the crust will be evanescent and nearly zero. We thus employed the WKB approximation to calculate approximate g -mode displacement fields and mode frequencies, assuming no propagation into the crust, and also use the resulting approximate p -mode dispersion relations in discussing the p -mode displacement fields in the core. First, we convert Eqs. (58,71–72,84) into two second-order equations for Π_n and Π_q , neglecting curvature terms, derivatives of the metric, f , the μ_{ab} and N_q , and ignoring entrainment. We obtain

$$\begin{aligned} \frac{d^2 \Pi_n}{dr^2} + \frac{d \ln n_n}{dr} \frac{d \Pi_n}{dr} + \left[-k_\perp^2 e^\lambda + \frac{\mu_0 \mu_{qq} e^{\lambda-\nu} \omega^2}{n_n D} \right] \Pi_n \\ = \frac{\mu_{nq} \mu_0 e^{\lambda-\nu} \omega^2}{n_n D} \Pi_q, \end{aligned} \quad (116)$$

$$\begin{aligned} \frac{d^2 \Pi_q}{dr^2} + \frac{d \ln n_q}{dr} \frac{d \Pi_q}{dr} + \left(1 - \frac{N_q^2}{\omega^2} \right) \left[-k_\perp^2 e^\lambda + \frac{\mu_0 \mu_{nn} e^{\lambda-\nu} \omega^2}{n_q D} \right] \Pi_q \\ = \frac{\mu_{nq} \mu_0 e^{\lambda-\nu} (\omega^2 - N_q^2)}{n_q D} \Pi_n, \end{aligned} \quad (117)$$

where we have used Eq. (76) to replace $d\mu_0/dr$. Defining $\Psi_a = \sqrt{n_a} \Pi_a$ and assuming that the Ψ_a have a slowly-varying amplitude $C_a(r)$ and a rapidly-oscillating phase $S(r) = \int k_r dr$. Inserting this definition into Eqs. (116–117) gives

$$(S')^2 C_n = M_{nn} C_n + M_{nq} C_q, \quad (118)$$

$$(S')^2 C_q = M_{qq} C_q + M_{qn} C_n, \quad (119)$$

where $d/dr = '$ and

$$M_{nn} = -k_\perp^2 e^\lambda + \frac{e^{\lambda-\nu} \omega^2 \mu_0 \mu_{qq}}{n_n D} - \frac{1}{\sqrt{n_n}} \frac{d^2 \sqrt{n_n}}{dr^2}, \quad (120)$$

$$M_{qq} = - \left(1 - \frac{N_q^2}{\omega^2} \right) k_\perp^2 e^\lambda + \frac{e^{\lambda-\nu} \omega^2 \mu_0 \mu_{nn}}{n_q D} - \frac{1}{\sqrt{n_q}} \frac{d^2 \sqrt{n_q}}{dr^2}, \quad (121)$$

$$M_{nq} = M_{qn} = - \frac{e^{\lambda-\nu} \omega^2 \mu_0 \mu_{nq}}{\sqrt{n_n n_q} D}. \quad (122)$$

Eqs. (118–119) have solutions

$$(S')^2 = \frac{1}{2} \left[(M_{nn} + M_{qq}) \pm \sqrt{(M_{nn} - M_{qq})^2 + 4M_{nq}^2} \right]. \quad (123)$$

As $|M_{nq}| \ll |M_{nn}|, |M_{qq}|$, we can identify a neutron-dominated mode with $(S')^2 = (k_r^2)_+ \approx M_{nn}$ and a charged fluid-dominated mode with $(S')^2 = (k_r^2)_- \approx M_{qq}$. In the low frequency $\omega^2 \lesssim N_q^2$ limit, $M_{nn} \sim -k_\perp^2 e^\lambda$, so the low-frequency neutron-dominated mode is nonpropagating. The charged fluid-dominated mode does propagate, however, since $M_{qq} \sim (N_q^2/\omega^2 - 1)k_\perp^2 e^\lambda$ in the low-frequency limit, thus giving a dispersion relation for the g -modes

$$\omega_g^2 \approx \frac{N_q^2 k_\perp^2 e^\lambda}{k^2}, \quad (124)$$

where $k^2 = k_r^2 + k_\perp^2 e^\lambda$, in agreement with the standard result of McDermott et al. (1983). The high frequency limit $\omega^2 \gg N_q^2$, keeping the M_{nq} contribution, gives the p -mode

dispersion relation in the crust

$$\omega_p^2 \approx c_{s\pm}^2 k^2, \quad c_{s\pm}^2 = e^{\nu-\lambda} \frac{n_n n_q}{2\mu_0} \left[\left(\frac{\mu_{qq}}{n_n} + \frac{\mu_{nn}}{n_q} \right) \pm \sqrt{\left(\frac{\mu_{qq}}{n_n} - \frac{\mu_{nn}}{n_q} \right)^2 + \frac{4\mu_{nq}^2}{n_n n_q}} \right], \quad (125)$$

suggesting two sets of p -modes, one associated with each superfluid. This is similar to the simplified p -mode dispersion relation given by [Passamonti et al. \(2016\)](#). Here we have implicitly assumed that the phases of the two fluids are the same. If the thermodynamic coupling μ_{nq} is ignored, Eq. (125) gives two completely separate dispersions, one for the charged fluid and one for the neutron fluid.

In the inner region of the star $r < r_t$, $k_r^2 < 0$ and the normal modes are exponentially damped. In the outer region $r_t < r < r_{\text{out}}$, $k_r^2 > 0$ and the modes are oscillatory. Matching at r_t with the exponential solution in the inner region and imposing $\Psi_a(r_{\text{out}}) = 0$ assuming no propagation into the crust, allowed g -modes will have k_r satisfying

$$\int_{r_t}^{r_{\text{out}}} k_r(r') dr' = \left(n_r - \frac{1}{4} \right) \pi, \quad n_r = 1, 2, 3, \dots, \quad (126)$$

where n_r is the radial node number. This condition determines the allowed frequencies since $k_r(r)$ is a function of ω . n_r here is the radial index of the solution, setting the radial node number for Ψ_a and by extension Π_a and ξ_a^r .

4.2 Numerical results

4.2.1 g -modes

To obtain solutions for the displacement fields ξ_a^i and the Π_a , we numerically integrated the system of four first-order equations given in the core by Eqs. (58), (71–72) and (84), in the crust by Eqs. (85), (87) and (95–96), and in the crust just above neutron drip by Eqs. (98–99). We use a standard energy normalization to set the amplitude of the displacement fields. Reinserting factors of c , this condition is

$$\frac{\omega^2}{c^2} \int_0^{R_{\text{cc}}} \int_{\Omega} dV \mu_0 \left[(1 - \epsilon_p) n_q \xi_q^{*i} \xi_i^q + (1 - \epsilon_n) n_n \xi_n^{*i} \xi_i^n + n_q \epsilon_p (\xi_q^{*i} \xi_i^n + \xi_n^{*i} \xi_i^q) \right] + \frac{\omega^2}{c^2} \int_{R_{\text{cc}}}^R \int_{\Omega} dV \mu_0 (n_f \xi_f^{*i} \xi_i^f + n_c \xi_c^{*i} \xi_i^c) = \frac{GM^2}{R}, \quad (127)$$

where M and R are the mass and radius of the star, R_{cc} is the coordinate radius of the crust-core transition, Ω indicates integration over the solid angle of a sphere and $dV = e^{\lambda/2} r^2 \sin \theta dr d\theta d\phi$. In the very thin single fluid region at densities just above neutron drip, $\xi_f^i = \xi_c^i = \xi_b^i$. Each function ($\xi_n^r, \xi_q^r, \xi_c^r, \xi_f^r, \Pi_n, \Pi_q, \Pi_c, \Pi_f, \xi_b^r, \Pi_n$) is scaled by the same amount, since they are all linearly related.

Figures 6 and 7 show the $l = 2$ g -mode frequency spectrum as a function of the stellar mass and the entrainment parameter ϵ_p , respectively, for the four different EOS parametrizations described in Table 1. The WKB frequencies for the $1.4M_{\odot}$ star with no entrainment are shown in Figure 7 to illustrate that they are extremely close to the exact frequencies for $n_{r,q} \gtrsim 2$, even though we did not permit propagation into the crust in the WKB approximation.

This indicates that the crust is largely unimportant to the mode frequency for the g -modes.

We find that our frequencies, which include general relativity, are redshifted compared to those of YW17. For example, they use the approximate g -mode frequency $\omega_g/2\pi \approx 590/n_{q,r}$ Hz for their $1.40M_{\odot}$, $m_p^*/m_N = 0.8$ and $K = 230.9$ MeV ([Rikovska Stone et al. 2003](#)) star, while we obtain an approximate frequency spectrum

$$\frac{\omega_g}{2\pi} \approx \frac{608 - 0.83(K - 240 \text{ MeV}) - 90 \frac{M}{M_{\odot}} + 297 \epsilon_p}{n_{r,q}} \text{ Hz}, \quad (128)$$

which is accurate to within $\lesssim 5\%$ for $n_{r,q} > 2$. This formula gives $\omega_g/2\pi \approx 549/n_{r,q}$ Hz for a $1.40M_{\odot}$, $\epsilon_p = 1 - m_p^*/m_N = 0.2$ and $K = 230.9$ MeV star in our model. Our frequencies are also lower than those of KG14, who did include general relativity. In this case, the differences in the frequencies are due to the different equations of state used, which also contributed to the differences between the results in this paper and those in YW17. Eq. 128 also indicates that the g -mode frequency is relatively insensitive to the nuclear compressibility K , with the numerator changing by only 41 Hz over the range of K values used here.

As expected from the $(1 + y) = (1 - Y(1 + \epsilon_p))/(1 - \epsilon_p - Y)$ proportionality of the Brunt–Väisälä frequency, the g -mode frequencies are increased as the entrainment parameter ϵ_p is increased. We find that the frequencies increase by a factor of ~ 1.4 from the $\epsilon = 0$ to the $\epsilon_p = 0.5$ values, in agreement with an expected scaling factor of $1/\sqrt{1 - \epsilon_p} = \sqrt{2}$ for low Y . However, we do not find an increase as large as found in YW17, with our frequencies with $\epsilon_p = 0.5$ being a factor of ~ 1.5 lower than theirs with $m_p^*/m_N = 0.4$. Possible reasons for the disagreement are the differences in the equation of state and in the structure of the star, which we compute by solving the TOV equation. The decrease in ω_g with K is also expected from the inverse relationship between N_q and K as seen in Figure 5, though this decrease is small (hence the relative insensitivity to K) because the g -modes can propagate over a longer distance in higher K stars due to their greater radii. The decrease in ω_g with M , even though the maximum value of N_q in the star increases with M , is explained as follows. Figure 4 shows that N_q becomes more peaked as a function of mass, meaning that the region of the star where k_r is real (between r_t and r_{out} in Eq. (126)) is smaller for large M . For large $n_{r,q}$ Eq. (126) becomes

$$\omega_g \approx \frac{l}{n_{r,q}\pi} \int_{r_t}^{r_{\text{out}}} \frac{N_q}{r} dr, \quad (129)$$

so ω_g is smaller for a particular $n_{r,q}$ when the range of integration is smaller, or when M is larger.

Figure 8 shows the displacement fields $\xi^r(r)$ and $\xi^{\perp}(r)$ for a few representative $l = 2$ g -modes in the $1.40M_{\odot}$ star. Since the leptonic Brunt–Väisälä frequency only acts on the charged fluid, the amplitude of the charged component is two orders of magnitude larger than the neutron component, and the neutron component is pulled along by the charge component through the thermodynamic coupling term μ_{nq} (and also by the entrainment if $\epsilon_p \neq 0$). In the crust, the g -mode frequencies are too low to excite oscillatory motion, and thus both the nuclear and neutron fluid displacements damp.

In the core, the charged component displacement fields

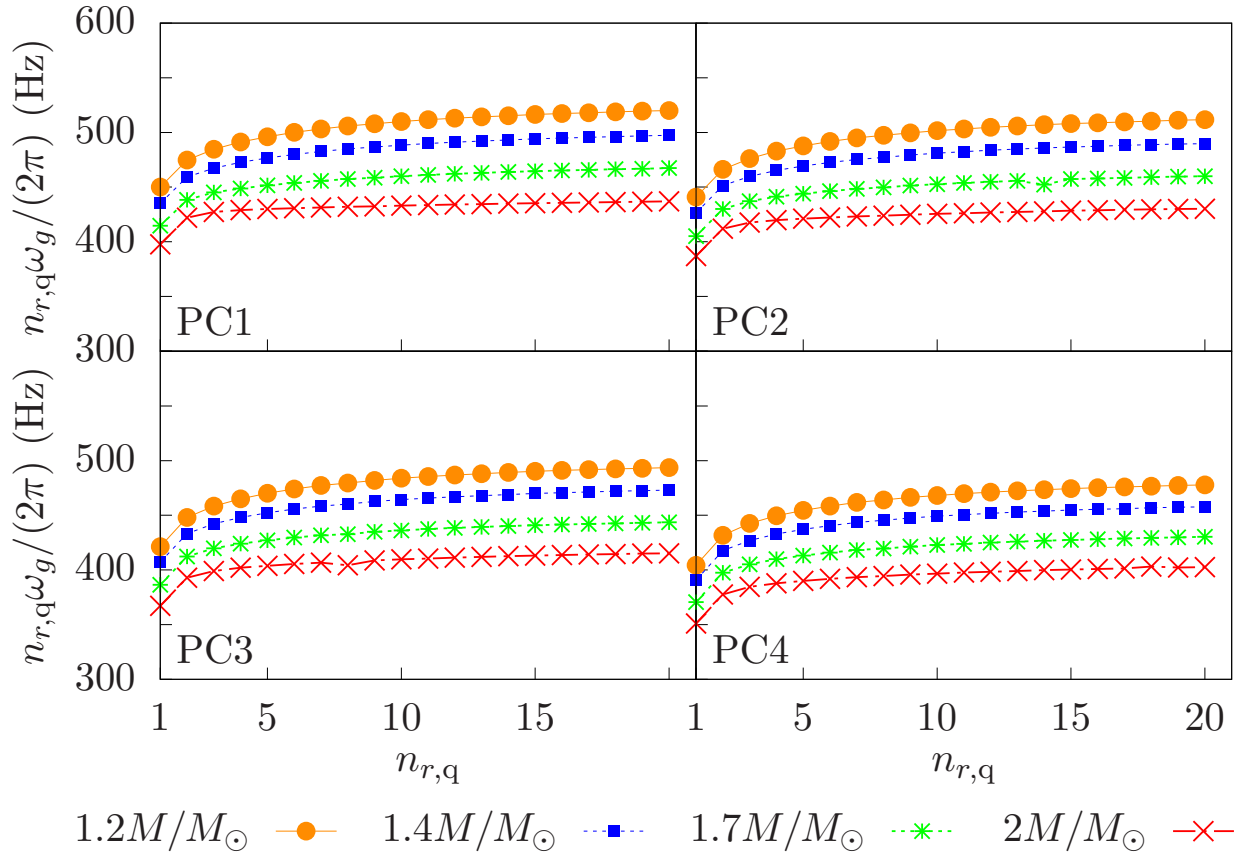


Figure 6. $l = 2$ g -mode (cyclical) frequencies for different values of the stellar mass and grouped by the EOS parametrization, denoted in the bottom left corner of each subplot. The entrainment in the core was set to zero when computing these frequencies.

are in reasonable agreement with YW17, but the neutron components have important differences. Our crust-core transition conditions change the oscillatory structure of the neutron component displacement fields, shifting them away from $\xi^r = 0$ in the outer part of the core. This justifies our specification of the g -modes using $n_{r,q}$, the radial node number of the charged fluid in the core. This is in contrast to results of YW17, which assumed a single normal fluid in the crust and imposes a crust-core transition condition (Eq. (B40) in YW17) that is equivalent to making both superfluid displacement fields equal. As the entrainment is increased in strength and the neutron fluid is forced to move along with the charged fluid to an even greater extent, we find that the radial nodes of the neutron fluid reappear at the locations of the charged fluid nodes. We cannot compare our results to YW17 in the crust because, unlike them, we treat the crust as two-fluids. We also do not compare our results to KG14, who do not show any displacement fields and who also use a single-fluid crust.

4.2.2 p -modes

Figure 9 shows four distinct $l = 2$ p -modes for a ϵ_p , $1.4M_\odot$ star, the first of which is actually an $n_r, n = n_{r,q} = 0$ f -modes. These illustrate that 1) there are twice as many p -modes

since there are two fluids, a result which is well-known (Lindblom & Mendell 1994; Lee 1995; Gualtieri et al. 2014), including multiple modes with the same radial node number for one or both fluids, and 2) the fluids need not oscillate in phase, meaning the n and q fluids can have different numbers of radial nodes. In fact, we find that, for $\epsilon_p = 0$, most of the p -modes for a two-superfluid star behave as if the two fluids are (almost) uncoupled. This agrees with previous work (Gusakov & Kantor 2011; Gualtieri et al. 2014). This means that the core WKB result Eq. (123) does not apply for all p -modes since it assumes that the two fluids have identical phase, which is not necessarily true. In contrast to the q -led g -modes, the amplitudes of the n and q -components of the p -modes are comparable. Additionally, the crust displacement fields can have multiple radial nodes, even with the crust constituting only a few percent of the star’s radial extent, since the wave number for the p -mode is often significantly smaller in the crust than in the core. Following Lindblom & Mendell (1994) we can classify p -modes by calculating the baryon current $Y\xi_q^r + (1 - Y)\xi_n^r$: those with small baryon current compared with $\xi_n^r - \xi_q^r$ are classified as superfluid modes, denoted “ s_i ”, while all others are classified as normal fluid modes, denoted “ p_i ”. This is similar to the classification scheme of Lindblom & Mendell (1994) and Lee (1995), who use a scheme based on quantities related to our Π_q and Π_n .

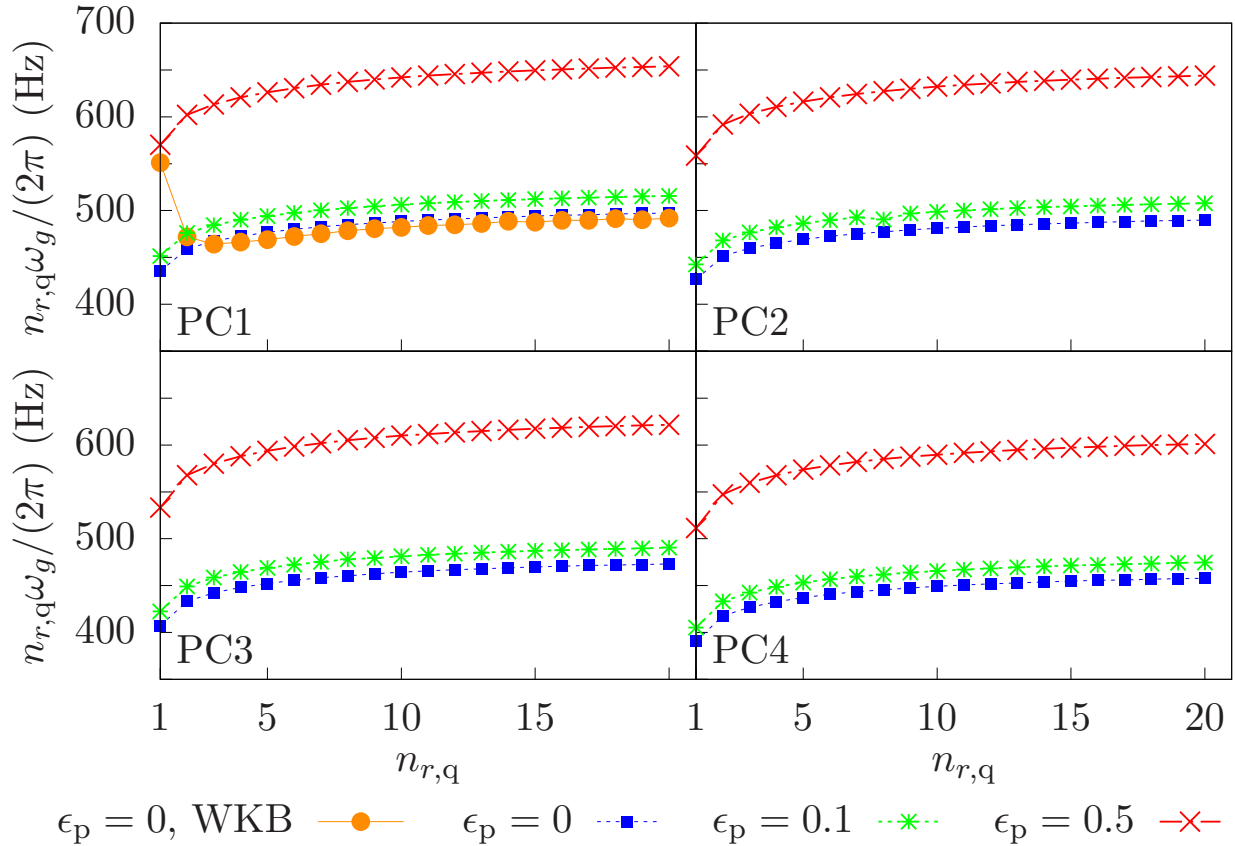


Figure 7. $l = 2$ g -mode (cyclical) frequencies for different values of the entrainment parameter ϵ_p , grouped by the EOS parametrization, denoted in the bottom left corner of each subplot. The WKB frequencies for a zero entrainment, $1.4M_\odot$ star with EOS parametrization PC1 is included in the upper left subplot. All stellar models used in this plot are of mass $1.4M_\odot$.

Figure 10 plots the radial node numbers in the core for each p -mode as a function of the mode frequency with zero entrainment. We plot $n_{r,n}$ and $n_{r,q}$ separately for modes in which they are not identical and only one of them for modes in which they are the same. The p -modes for which $n_{r,n} \neq n_{r,q}$ the two components of the mode each roughly obey the uncoupled fluid dispersion relations $k_r^n \approx M_{nn}$ and $k_r^q \approx M_{qq}$, and those which have $n_{r,n} = n_{r,q}$ and roughly obey one of the two (coupled) WKB results given by Eq. (123). The modes of the latter type are labeled distinctly based on which solution $(k_r)_\pm$ they follow most closely. The separate, uncoupled dispersion relations obeyed by most p -modes suggest that they are formed from separate n and q oscillations which are paired together through the weak thermodynamic coupling (in the case of zero entrainment) due to having similar frequencies, with the pairing shifting the mode away from either of the exact frequencies that the uncoupled fluid modes would have. This means that the n and q components of each mode are not required to have the same node number, which is what we observe. The frequency residuals $\Delta\omega_p$ compared to the uncoupled fluid or WKB result are shown in the right panel. For the nearly uncoupled modes, these were obtained by comparing the numerically calculated frequency to the expected frequency for the separate fluid components for a

given $n_{r,n}$ or $n_{r,q}$ as calculated using $k_r^n \approx M_{nn}$ and $k_r^q \approx M_{qq}$ and Eq. (126). For the $n_{r,n} = n_{r,q}$ modes, the expected frequency was calculated for a given n_r by using Eq. (126) and the WKB solution from Eq. (123) which gave the smallest frequency difference for each mode. $\Delta\omega_p$ is small for most modes, indicating that they are well-described by either the nearly uncoupled or standard WKB dispersions. Many of the residuals for the high-frequency uncoupled-type neutron fluid modes are large, suggesting that for these modes the charged part of the mode could be “pulling” the neutron part towards being an $n_{r,n} = n_{r,q}$, charged fluid-like mode obeying the dispersion relation $(k_r)_-$.

We also calculated the p -modes for a $1.40M_\odot$ star with strong entrainment $\epsilon_p = 0.5$. As expected, this drastic increase in the entrainment reduces the difference in the radial node number between the two fluids to at most ± 1 . It additionally tries to force the modes to obey the neutron-dominated WKB dispersion $(k_r)_+ \approx M_{nn}$, which is shown in Figure (11). That it is this solution that is selected as opposed to the charged fluid-dominated one suggests that the p -modes can be thought of as neutron-dominated in the same way that the g -modes can be considered charge-fluid dominated, with this shift arising because the entrainment coefficient in the neutron equations $\epsilon_n = n_q/n_n\epsilon_p$ is about an

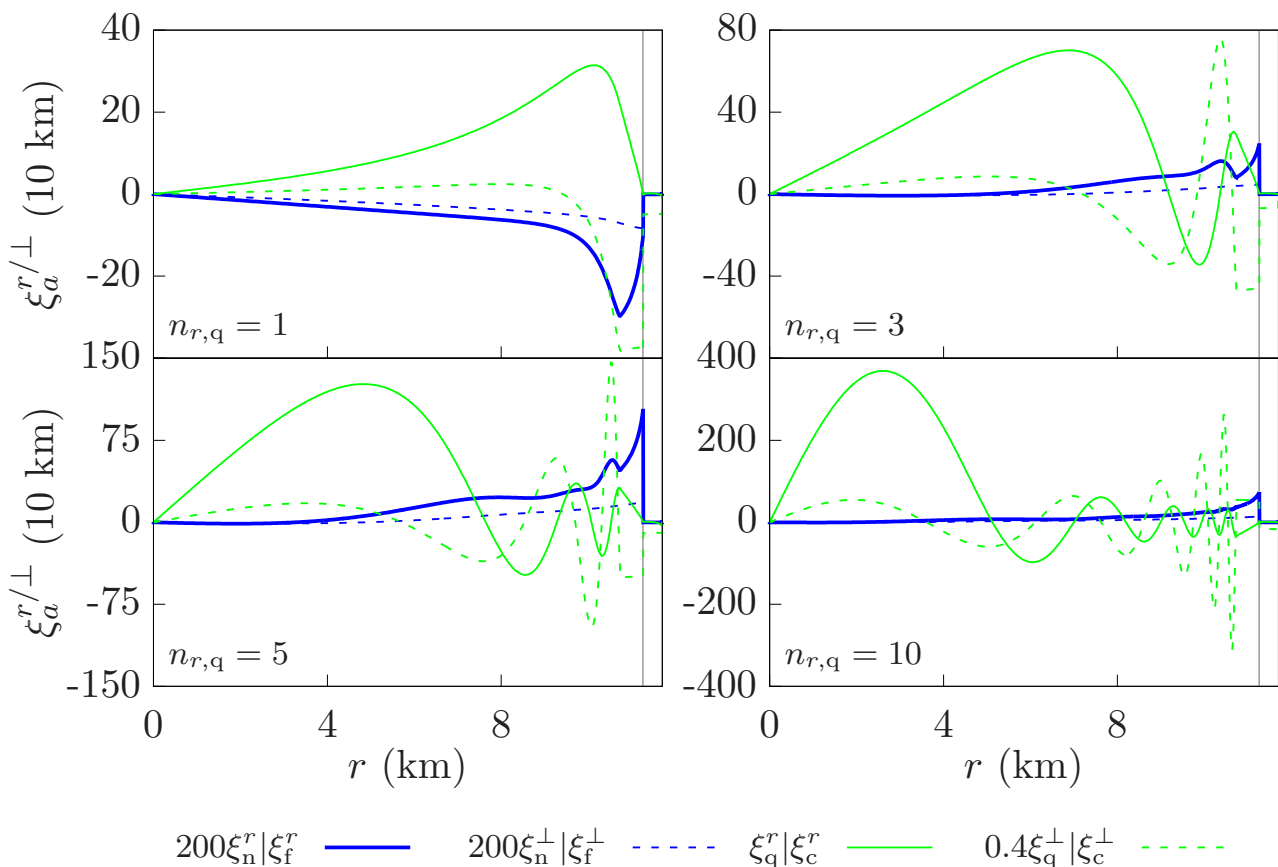


Figure 8. Displacement fields ξ^r and ξ^\perp for four $l = 2$ g -modes in a $1.40M_\odot$, zero entrainment star with EOS parametrization PC1: $(n_{r,q}, \omega/2\pi) = (1, 435.2 \text{ Hz})$, $(3, 155.8 \text{ Hz})$, $(5, 95.34 \text{ Hz})$ and $(10, 48.84 \text{ Hz})$. The crust-core interface is indicated by the thin line at 11.27 km. To the left of this line, the displacement fields are $(\xi_n^r, \xi_q^r, \xi_n^\perp, \xi_q^\perp)$, while to the right they are $(\xi_f^r, \xi_c^r, \xi_f^\perp, \xi_c^\perp)$. (ξ_b^r, ξ_b^\perp) , which do not vary much over the very thin region ($\sim 10 \text{ m}$) of single fluid above neutron drip, are not shown.

order of magnitude smaller than ϵ_p , which appears in the charged fluid equations.

A final point of interest concerning the p -modes is the possible existence of pairs of distinct p -modes which are closely-spaced in frequency, as opposed to the nearly uniformly-spaced in frequency p -modes expected in the single fluid or WKB two-fluid cases. An example of such a mode pair we found for the $1.40M_\odot$, $K = 230 \text{ MeV}$, $\epsilon_p = 0$ star is the pair $(n_{r,q} = 6, n_{r,n} = 6, \omega_p/2\pi = 24116 \text{ Hz})$ and $(n_{r,q} = 10, n_{r,n} = 9, \omega_p/2\pi = 24264 \text{ Hz})$, which have a frequency spacing of the order of the g -mode frequencies. A similar phenomenon is observed in the finite temperature calculation of Gualtieri et al. (2014), where the p -mode frequencies become very similar at certain “resonance” temperatures, though our results indicate that nearly-resonant p -modes can occur at any temperature. These mode pairs could provide a source of large nonlinear mode couplings for the two-superfluid version of the p - g instability discussed in recent papers (Weinberg et al. 2013; Venumadhav et al. 2014; Weinberg 2016). These instabilities may be observable through phase shifts in the gravitational waveforms of binary neutron star mergers (Essick et al. 2016; Andersson & Ho 2018).

5 CONCLUSIONS

We have calculated the g - and p -modes of a superfluid star with leptonic buoyancy using a specific model for nuclear matter in the core and the crust. We have included general relativity and a two-fluid crust when computing the normal modes, finding that the crust-core interface conditions for the displacement fields change the neutron components of the g -mode displacement fields in the core by removing many of their radial nodes. In order to compute the modes, we have developed a simple but flexible equation of state for both crust and core which contains all of the thermodynamics required by our formalism. This allowed us to compute oscillation modes for a range of stellar and nuclear physics parameters, and our EOS can be easily adjusted to agree with new neutron star or nuclear physics measurements. In general our leptonic buoyancy g -mode frequencies are similar to those found previously, considering differences in the equations of state used to model the star and redshift factors, and are dominated by the charged fluid in which the buoyancy exists. We find that the g -mode frequencies increase with entrainment and decrease with stellar mass and nuclear compressibility, with only weak dependence on the latter. Our decomposition of the fluid into neutron and charged

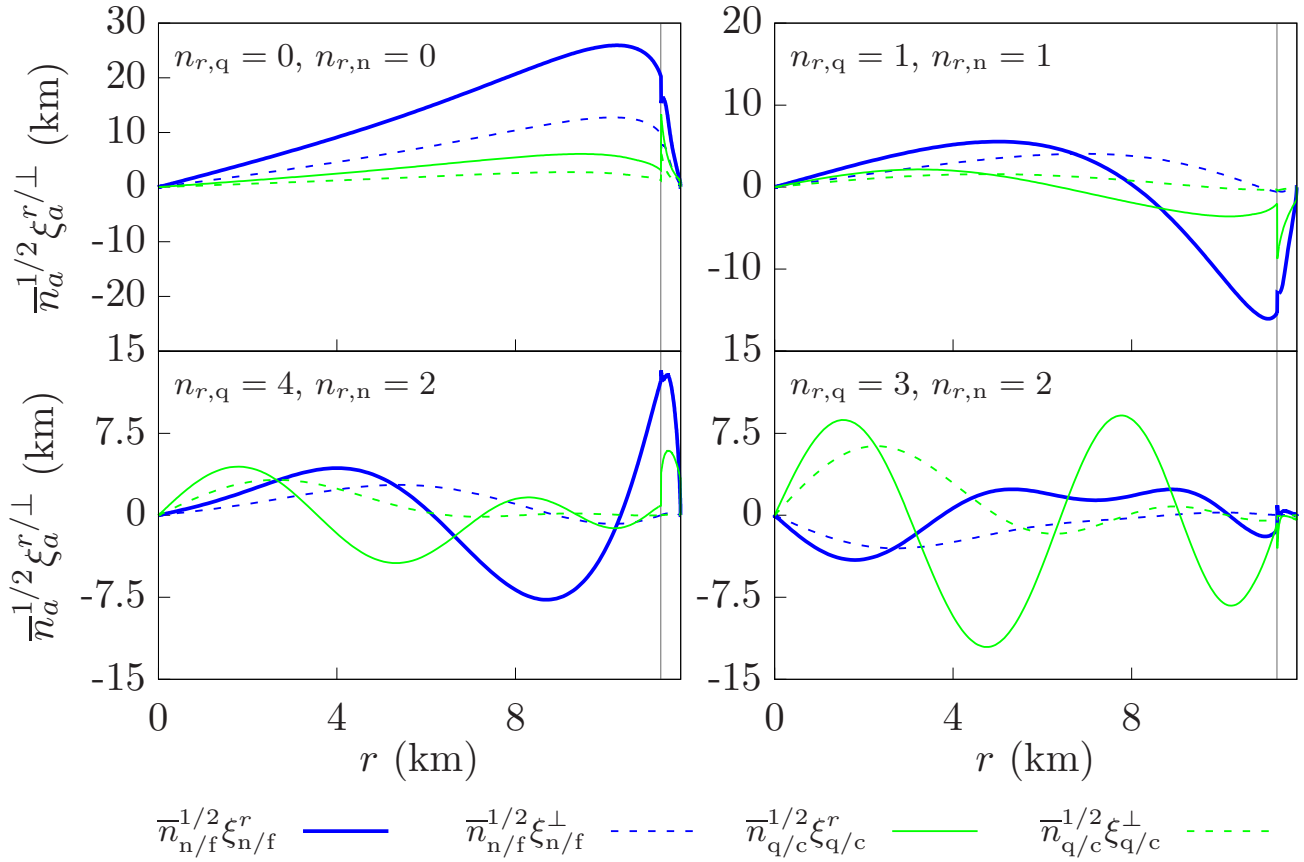


Figure 9. Displacement fields ξ^r and ξ^\perp for the $l = 2$ f -mode and three p -modes in a $1.40M_\odot$, zero entrainment star: $(x_i, n_{r,q}, n_{r,n}, \omega_g/2\pi) = (f, 0, 0, 2302 \text{ Hz})$, $(p_1, 1, 1, 6576 \text{ Hz})$, $(p_2, 4, 2, 9703 \text{ Hz})$ and $(s_3, 3, 2, 10378 \text{ Hz})$, where x_i refers to the standard classification of the mode and its order as a subscript. The crust-core interface is indicated by the thin line at 11.27 km. To the left of this line, the displacement fields are $(\xi_n^r, \xi_n^\perp, \xi_q^r, \xi_q^\perp)$, while to the right they are $(\xi_f^r, \xi_f^\perp, \xi_c^r, \xi_c^\perp)$. (ξ_b^r, ξ_b^\perp) , which do not vary much over the very thin region (~ 10 m) of single fluid above neutron drip, are not shown. The radial node numbers $n_{r,q}$ and $n_{r,n}$ for each fluid for each mode are indicated in the upper left of each plot. The displacement fields have been scaled by factors of $\bar{n}_a^{1/2} = (n_a/n_{\text{nuc}})^{1/2}$, which accounts for the abrupt jumps occurring at the crust-core transition.

components clearly illustrates that the neutrons are pulled along by the charged fluid in the g -modes through thermodynamic coupling and entrainment, and otherwise would not participate in the g -mode.

In contrast, for zero entrainment, we reproduce earlier results (Gusakov & Kantor 2011; Gualtieri et al. 2014) that most of the p -modes behave as nearly uncoupled fluids, with the weak coupling between the two superfluids leading to pairing between uncoupled n - and q -fluid modes with similar frequencies. This results in p -modes whose charged and neutron components can have widely-differing radial node numbers, and in p -modes with frequency differences on the order of the g -mode frequencies. These could thus contribute to the recently proposed tidal- p - g or related instabilities which depends on nonlinear couplings between p and g -modes. For large entrainment, we find “neutron-dominated” p -modes, in which the phases of the two superfluids in the core are nearly the same so that they almost behave as a single neutron fluid.

As mentioned briefly by YW17 and incorporated in a recent paper (Yu & Weinberg 2017b), we should include hyper-

ons in the neutron star core, as the chemical potential above $\sim 3n_{\text{nuc}}$ reaches the bare rest mass of the Λ hyperon. This will lead to a softening of the equation of state and may provide additional hyperon superfluids which couple thermodynamically to the neutron and charged fluids, or if the hyperons are not superfluid, a hyperonic Brunt–Väisälä frequency which can modify the g -modes in the inner core (Dommes & Gusakov 2016). If the star is able to contain Ξ^- hyperons it could have a hyperonic Brunt–Väisälä frequency even if the hyperons are superfluid, since the Ξ^- would be expected to comove with the protons to which they are electrostatically coupled. Such hyperonic buoyancy would shift the g -mode frequencies obtained from leptonic buoyancy alone, which could be used as an indicator of the presence of hyperons in neutron stars if the resulting gravitational waveform phase shifts from the resonant excitation of these g -modes in binary neutron star inspirals could be measured. However, if the EOS is softened too much by the hyperons, it could become difficult for it to allow stars of mass $> 2M_\odot$, as reaching this mass already required large nuclear compressibilities or high central densities.

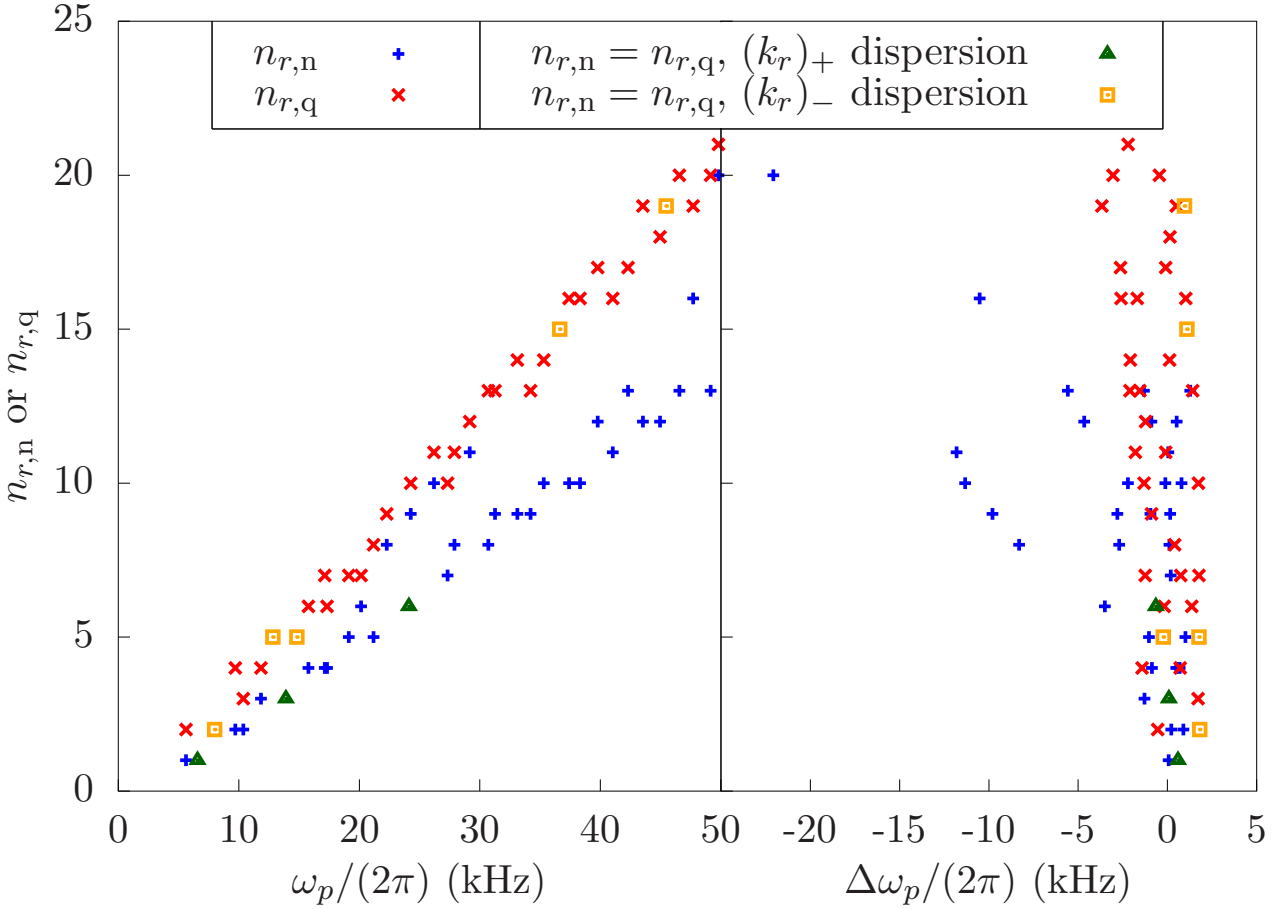


Figure 10. Left: $l = 2$ p -mode radial node numbers $n_{r,n}$ and $n_{r,q}$ plotted as a function of the frequency of the corresponding mode for a $1.40M_{\odot}$, zero entrainment star. The f and s_0 ($\omega/2\pi = 28687$ Hz) modes are not shown. Modes where $n_{r,n} \neq n_{r,q}$ have the radial node numbers of the n and q displacement fields denoted separately, but are paired i.e. there are two ticks at the same frequency ω_p , one (+) denoting the value of $n_{r,n}$ and the other (x) denoting $n_{r,q}$. Modes where $n_{r,n} = n_{r,q}$ are denoted by distinct symbols depending on whether they more closely follow the $(k_r)_+$ (n -dominated, denoted by a triangle) or $(k_r)_-$ (q -dominated, denoted by a square) WKB dispersion relation. Right: Residuals $\Delta\omega_p$ between the full numerically calculated p -mode frequencies and those that an uncoupled n or q mode of identical $n_{r,n}/n_{r,q}$ would have (for $n_{r,n} \neq n_{r,q}$) or between the fully numerically calculated p -mode frequencies and the nearest coupled WKB frequency corresponding to the same radial node number $n_{r,n} = n_{r,q}$.

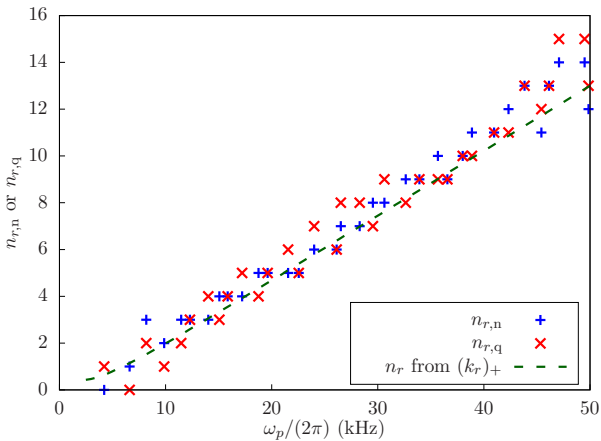


Figure 11. p -modes for $1.40M_{\odot}$, $\epsilon_p = 0.5$ star with parametrization PC1 for the EOS, and n_r (including fractional values) as a function of ω determined from Eq. (126) using $(k_r)_+ \approx M_{nn}$.

ACKNOWLEDGEMENTS

This work was supported in part by NASA ATP grant NNX13AH42G. PBR was also supported in part by the Boochever Fellowship at Cornell for fall 2017. We also thank the referee for many helpful comments that improved our paper.

REFERENCES

- Abbott B., et al., 2017, *Phys. Rev. Lett.*, 119, 161101
 Agathos M., Meidam J., Del Pozzo W., Li T. G., Tompitak M., Veitch J., Vitale S., Van Den Broeck C., 2015, *Phys. Rev. D*, 92, 023012
 Andersson N., Comer G. L., 2007, *Living Rev. Relativ.*, 10, 1
 Andersson N., Ho W. C., 2018, *Phys. Rev. D*, 97, 23016
 Andersson N., Haskell B., Samuelsson L., 2011, *Mon. Not. R. Astron. Soc.*, 416, 118
 Antoniadis J., et al., 2013, *Science* (80-.), 340, 1233232
 Baldo M., Schulze H. J., 2007, *Phys. Rev. C*, 75, 025802

Baym G., Pethick C., Sutherland P., 1971a, *Astrophys. J.*, 170, 299

Baym G., Bethe H. A., Pethick C. J., 1971b, *Nucl. Physics, Sect. A*, 175, 225

Bertoni B., Reddy S., Rrapaj E., 2015, *Phys. Rev. C*, 91, 025806

Bildsten L., Cutler C., 1992, *Astrophys. J.*, 400, 175

Bildsten L., Cutler C., 1995, *Astrophys. J.*, 449, 800

Carter B., Langlois D., 1998, *Nucl. Phys. B*, 531, 478

Chamel N., 2017, *J. Low Temp. Phys.*, 189, 328

Cutler C., et al., 1993, *Phys. Rev. Lett.*, 70, 2984

Dommes V. A., Gusakov M. E., 2016, *Mon. Not. R. Astron. Soc.*, 455, 2852

Douchin F., Haensel P., 2000, *Phys. Lett. B*, 485, 107

Epstein R. I., 1988, *Astrophys. J.*, 333, 880

Essick R., Vitale S., Weinberg N. N., 2016, *Phys. Rev. D*, 94, 103012

Flanagan É. É., Racine É., 2007, *Phys. Rev. D*, 75, 044001

Gezerlis A., Carlson J., 2010, *Phys. Rev. C*, 81, 025803

Gezerlis A., Pethick C. J., Schwenk A., 2014, in Bannemann K. H., Kettererson J. B., eds., *Novel Superfluids*, Volume 2. Oxford University Press, Oxford, Chapt. 22, pp 580–616

Gualtieri L., Kantor E. M., Gusakov M. E., Chugunov A. I., 2014, *Phys. Rev. D*, 90, 024010

Gusakov M. E., Kantor E. M., 2011, *Phys. Rev. D*, 83, 081304

Gusakov M. E., Kantor E. M., 2013, *Phys. Rev. D*, 88, 101302

Haensel P., 2001, in Blaschke D., Glendenning N. K., Sedrakian A., eds., *Physics of Neutron Star Interiors*. Springer, Berlin, Chapt. 5, pp 127–174

Hashimoto M., Seki H., Yamada M., 1984, *Prog. Theor. Phys.*, 71, 320

Hebeler K., Lattimer J. M., Pethick C. J., Schwenk A., 2013, *Astrophys. J.*, 773

Ho W. C. G., Lai D., 1999, *Mon. Not. R. Astron. Soc.*, 308, 153

Kantor E. M., Gusakov M. E., 2014, *Mon. Not. R. Astron. Soc. Lett.*, 442, 90

Kobyakov D., Pethick C. J., 2013, *Phys. Rev. C*, 87, 055803

Kobyakov D., Pethick C. J., 2016, *Phys. Rev. C*, 94, 055806

Lackey B. D., Wade L., 2015, *Phys. Rev. D*, 91, 043002

Lai D., 1994, *Mon. Not. R. Astron. Soc.*, 270, 611

Lattimer J. M., Prakash M., 2016, *Phys. Rep.*, 621, 127

Lattimer J. M., Pethick C. J., Ravenhall D. G., Lamb D., 1985, *Nucl. Phys. A*, 432, 646

Lee U., 1995, *Astron. Astrophys.*, 303, 515

Lindblom L., Mendell G., 1994, *Astrophys. J.*, 421, 689

Lombardo U., Schulze H.-J., 2001, in Blaschke D., Glendenning N. K., Sedrakian A., eds., *Physics of Neutron Star Interiors*. Springer, Berlin, Chapt. 2, pp 30–53

McDermott P., Van Horn H., Scholl J., 1983, *Astrophys. J.*, 268, 837

Onsi M., Dutta A. K., Chatri H., Goriely S., Chamel N., Pearson J. M., 2008, *Phys. Rev. C*, 77, 062805

Page D., Prakash M., Lattimer J. M., Steiner A. W., 2011, *Phys. Rev. Lett.*, 106, 081101

Passamonti A., Andersson N., 2012, *Mon. Not. R. Astron. Soc.*, 419, 638

Passamonti A., Andersson N., Ho W. C. G., 2016, *Mon. Not. R. Astron. Soc.*, 455, 1489

Pearson J. M., Chamel N., Goriely S., Ducoin C., 2012, *Phys. Rev. C*, 85, 065803

Potekhin A. Y., Fantina A. F., Chamel N., Pearson J. M., Goriely S., 2013, *Astron. Astrophys.*, 560, A48

Prix R., Rieutord M., 2002, *Astron. Astrophys.*, 393, 949

Ravenhall D. G., Bennett C. D., Pethick C. J., 1972, *Phys. Rev. Lett.*, 28, 978

Ravenhall D. G., Pethick C. J., Wilson J. R., 1983a, *Phys. Rev. Lett.*, 50, 2066

Ravenhall D. G., Pethick C. J., Lattimer J. M., 1983b, *Nucl. Phys. A*, 407, 571

Reisenegger A., Goldreich P., 1992, *Astrophys. J.*, 395, 240

Reisenegger A., Goldreich P., 1994, *Astrophys. J.*, 426, 688

Rikovska Stone J., Miller J. C., Koncewicz R., Stevenson P. D., Strayer M. R., 2003, *Phys. Rev. C*, 68, 16

Venumadhav T., Zimmerman A., Hirata C. M., 2014, *Astrophys. J.*, 781, 23

Watanabe G., Sato K., Yasuoka K., Ebisuzaki T., 2003, *Phys. Rev. C*, 68, 21

Weinberg N. N., 2016, *Astrophys. J.*, 819, 109

Weinberg N. N., Arras P., Burkart J., 2013, *Astrophys. J.*, 769, 121

Xu W., Lai D., 2017, *Phys. Rev. D*, 96, 083005

Yakovlev D. G., Levenfish K. P., Shibano Y. A., 1999, *Rev. Top. Probl.*, 42, 737

Yu H., Weinberg N. N., 2017a, *Mon. Not. R. Astron. Soc.*, 464, 2622

Yu H., Weinberg N. N., 2017b, *Mon. Not. R. Astron. Soc.*, 470, 350

Zhou X. R., Schulze H. J., Zhao E. G., Pan F., Draayer J. P., 2004, *Phys. Rev. C*, 70, 048802

APPENDIX A: CALCULATION OF CHEMICAL POTENTIAL DERIVATIVES IN THE CRUST

Computing μ_{ff} , μ_{cc} and μ_{fc} is more complicated than finding the μ_{ab} in the core. In the core, the energy density is a function of three variables, chosen to be (n_n, n_q, f) or $(n_b, Y = n_q/n_b, f)$. In the background, chemical equilibrium relates Y and f to n_b ; in perturbations, chemical equilibrium fails. In the crust, the energy density depends on five variables, three of which describe nuclei: (A, n_i, Y) . In equilibrium, there are four conditions that permit computing A , n_i , Y and n_c (or $Y_c \equiv n_c/n_b$) as functions of n_b ; for perturbations, there are still three conditions, which may be solved in principle to find $A(n_f, n_c)$, $n_i(n_f, n_c)$ and $Y(n_f, n_c)$, which we would then need to differentiate to compute μ_{ab} $a, b \in \{f, c\}$.

Fortunately, perturbations away from equilibrium are small, so we only need to find the energy density ρ as a function of (n_b, Y_c) near equilibrium to compute μ_{ab} . Define

$$\Delta Y_c = Y_c - Y_c^{\text{eq}}(n_b), \quad (\text{A1})$$

where $Y_c^{\text{eq}}(n_b)$ is the equilibrium value of Y_c and $\Delta Y_c = 0$ in equilibrium. Then near but not in equilibrium, the energy density is

$$\rho(n_b, Y_c) = \rho_{\text{eq}}(n_b) + \frac{1}{2} C(n_b) (\Delta Y_c)^2, \quad (\text{A2})$$

where $\rho_{\text{eq}}(n_b)$ is evaluated in the background and

$$C(n_b) (\Delta Y_c)^2 = \sum_{i,j} \left(\frac{\partial^2 \rho(n_b, Y_c, A, Y, n_i)}{\partial X_i \partial X_j} \right) \Delta X_i \Delta X_j, \quad (\text{A3})$$

where $X_i = A, Y, n_i, Y_c$.

Perturbed fluid elements will quickly reach mechanical equilibrium and partial chemical equilibrium (i.e. not beta equilibrium) with their surroundings and will obey the “nuclear virial theorem”. These conditions are expressed as

$$E_{\text{Coul}} = 2E_{\text{surf}} \quad (\text{A4})$$

$$\mu_{n,i} - \mu_{n,o} = \frac{4\pi r_n^2 Y}{A} \frac{d\sigma_s}{dY}, \quad (\text{A5})$$

$$P_{i,\text{bulk}} - P_{o,\text{bulk}} = \frac{2\sigma_s}{r_n} - \frac{4\pi}{15} (Y n_i r_n e)^2 (1 - w), \quad (\text{A6})$$

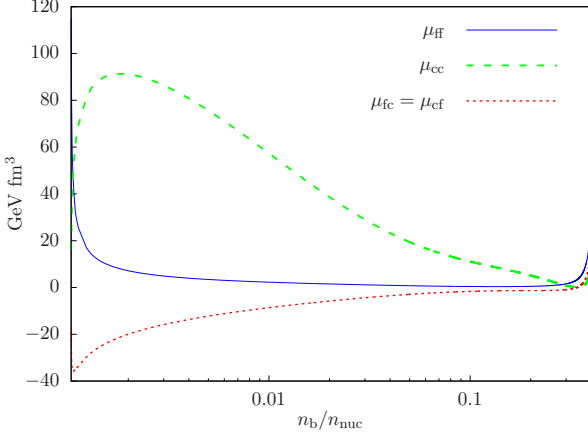


Figure A1. Thermodynamic derivatives in the crust μ_{ff} , μ_{cc} and μ_{fc} as a function of the baryon density $0.00104 < n_{\text{b}}/n_{\text{nuc}} < 0.394$ for the PC1 parametrization of our EOS.

where we have defined

$$\mu_{\text{n},\text{i}} \equiv \frac{\partial \rho_{\text{bulk},\text{i}}}{\partial (n_{\text{i}}(1-Y))}, \quad (\text{A7})$$

$$\mu_{\text{n},\text{o}} \equiv \frac{\partial \rho_{\text{bulk},\text{o}}}{\partial n_{\text{n},\text{o}}}, \quad (\text{A8})$$

$$P_{\text{i},\text{bulk}} \equiv n_{\text{i}}^2 \frac{\partial}{\partial n_{\text{i}}} \left(\frac{\rho_{\text{bulk},\text{i}}}{n_{\text{i}}} \right), \quad (\text{A9})$$

$$P_{\text{o},\text{bulk}} \equiv n_{\text{n},\text{o}}^2 \frac{\partial}{\partial n_{\text{n},\text{o}}} \left(\frac{\rho_{\text{bulk},\text{o}}}{n_{\text{n},\text{o}}} \right). \quad (\text{A10})$$

The perturbed fluid elements will not be in beta equilibrium with their surroundings, since the weak interaction timescale is much longer than the timescale of the fluid oscillations, so $\partial \rho / \partial Y \neq 0$. We then use Eqs. (A4–A6) to relate ΔY_{c} to ΔA , ΔY and Δn_{i} as in Eq. (A3) taking the differential of these three equations gives

$$0 = \rho_{AA} \Delta A + \rho_{An_{\text{i}}} \Delta n_{\text{i}} + \rho_{AY} \Delta Y + \rho_{AY_{\text{c}}} \Delta Y_{\text{c}}, \quad (\text{A11})$$

$$0 = \rho_{n_{\text{i}}n_{\text{i}}} \Delta n_{\text{i}} + \rho_{An_{\text{i}}} \Delta A + \rho_{Yn_{\text{i}}} \Delta Y + \rho_{n_{\text{i}}Y_{\text{c}}} \Delta Y_{\text{c}}, \quad (\text{A12})$$

$$0 = \rho_{Y_{\text{c}}Y_{\text{c}}} \Delta Y_{\text{c}} + \rho_{n_{\text{i}}Y_{\text{c}}} \Delta n_{\text{i}} + \rho_{AY_{\text{c}}} \Delta A + \rho_{YY_{\text{c}}} \Delta Y, \quad (\text{A13})$$

where $\rho_{X_i X_j} \equiv \partial^2 \rho / (\partial X_i \partial X_j)$. Eq. (A2) then gives the thermodynamic derivatives μ_{bb} , $\mu_{Y_{\text{c}}Y_{\text{c}}}$ and $\mu_{\text{b}Y_{\text{c}}} = \mu_{Y_{\text{c}}\text{b}}$ as

$$\mu_{\text{bb}} = \frac{d^2 \rho_{\text{eq}}}{dn_{\text{b}}^2} + C(n_{\text{b}}) \left(\frac{dY_{\text{c}}^{\text{eq}}}{dn_{\text{b}}} \right)^2, \quad (\text{A14})$$

$$\mu_{Y_{\text{c}}Y_{\text{c}}} = C(n_{\text{b}}), \quad (\text{A15})$$

$$\mu_{\text{b}Y_{\text{c}}} = -C(n_{\text{b}}) \frac{dY_{\text{c}}^{\text{eq}}}{dn_{\text{b}}}, \quad (\text{A16})$$

using which μ_{cc} , μ_{ff} and $\mu_{\text{fc}} = \mu_{\text{cf}}$ are found using Eqs. (54–56), replacing $Y \rightarrow Y_{\text{c}}$, $q \rightarrow c$ and $n \rightarrow f$. The expressions for μ_{cc} , μ_{ff} and μ_{fc} are quite complicated and are not given explicitly here, but they are plotted in Figure A1 for the PC1 parametrization of our EOS.

This paper has been typeset from a $\text{\TeX}/\text{\LaTeX}$ file prepared by the author.